Biogeosciences Discuss., 8, 8091–8160, 2011
www.biogeosciences-discuss.net/8/8091/2011/
doi:10.5194/bgd-8-8091-2011

Biogeosciences Discussions

The Biogeochemistry from the Oligotrophic to the Ultraoligotrophic Mediterranean (BOUM) experiment

T. Moutin[1], F. Van Wambeke[2], and L. Prieur[3]

[1]INSU-CNRS, Laboratoire d'Océanographie Physique et Biogéochimique (LOPB), UMR6535, CNRS-IRD-Université de la Méditerranée, Centre d'Océanologie de Marseille, Campus de Luminy, Case 901, 13288 Cedex 09 Marseille, France
[2]INSU-CNRS, Laboratoire de Microbiologie, Géochimie et Ecologie Marines, UMR6117, Centre d'Océanologie de Marseille, Aix Marseille Université, France
[3]INSU-CNRS, Laboratoire d'Océanographie de Villefranche, UMR7093, Université Paris VI, Villefranche sur mer, France

Received: 1 August 2011 – Accepted: 2 August 2011 – Published: 10 August 2011

Correspondence to: T. Moutin (thierry.moutin@univmed.fr)

Published by Copernicus Publications on behalf of the European Geosciences Union.

Abstract

The overall goal of the BOUM (Biogeochemistry from the Oligotrophic to the Ultra-oligotrophic Mediterranean) experiment was to obtain a better representation of the interactions between planktonic organisms and the cycle of biogenic elements in the Mediterranean Sea (MS), in the context of global climate change and, more particularly, on the role of the ocean in carbon sequestration through biological processes. The BOUM experiment was organized around three main objectives which are: (1) to give a longitudinal description of the biogeochemistry and the biological diversity of the MS during the strongest stratified period, (2) to study processes at the centre of three anticyclonic eddies, and (3) to obtain a representation of the main biogeochemical fluxes and the dynamics of the planktonic trophic network. The international BOUM cruise took place between 16 June and 20 July 2008, involved 32 scientists on board, and covered around 3000 km in the MS from the South of Cyprus to Marseilles (France). This paper describes in detail the objectives of the BOUM experiment, the implementation plan of the cruise, the water masses and general biogeochemical trends encountered, and lays particular emphasis on description of the sections and the main physical characteristics of the three anticyclonic eddies studied, before concluding with first order biogeochemical budgets and a general overview of the 24 other papers published in this special issue.

1 Introduction

The additional CO_2 in the atmosphere, mainly resulting from fossil fuel emissions linked to human activities (anthropogenic CO_2), is the main cause of global warming. The ocean has acted as a major sink of anthropogenic CO_2 (Sabine et al., 2004) preventing a greater accumulation in the atmosphere and therefore a greater increase in the earth temperature. Although the biological pump (Fig. 1) provides the main explanation for the vertical gradient of carbon in the ocean, it was thought to be in an equilibrium state

BGD
8, 8091–8160, 2011

with an associated near zero net exchange of CO_2 with the atmosphere (Broecker, 1991; Murname et al., 1999). Climate alterations are beginning to disrupt this equilibrium and the expected modification of the biological pump will probably considerably influence oceanic carbon sequestration (and therefore global warming) over a decadal time scale (Sarmiento and Grüber, 2006).

CO_2 is exchanged at the atmosphere-ocean interface and reacts with carbonate ions. The timescale for reaching equilibrium within the upper layer is about a year (Kleypas and Langdon, 2006). This dissolved inorganic carbon is then transported much more slowly into deeper layers via mixing. This second step limits the sequestration of anthropogenic CO_2 in the ocean on a decadal time scale and therefore, influences the accumulation of CO_2 in the atmosphere and thus, subsequent climate alteration (Sarmiento and Grüber, 2006). Some of the CO_2 in the upper layer is incorporated into biomass by photosynthesis. This synthesis of particulate organic carbon is essentially dependent on the availability of light and nutrients (including trace metals). A fraction of the particulate organic carbon pool is transferred into the dissolved organic pool (Maranon et al., 2005). Most of the organic carbon is recycled in the upper surface layer and the CO_2 produced is re-exchanged with the atmosphere over a short time scale. Only a fraction of the organic carbon is exported to the ocean interior and constitutes the biological pump (Fig. 1).

Predictions in the 21st century seem to indicate an oligotrophication of the open ocean, resulting in a weakening of the transfer of carbon to the ocean interior and a concomitant acceleration of climate change (Boyd and Doney, 2003; Le Quéré et al., 2009). In order to determine the actual efficiency of the biological pump and to forecast its future efficiency, major challenges today concern both biogeochemical, physical and biological oceanography. Major questions arise, of which one is central: what is the balance between production of organic matter in the photic layer, and remineralisation in the upper layer?

What are the main processes controlling the vertical exchanges of nutrients and organic matter and particularly, what is the role of mesoscale activity and its links with

BGD
8, 8091–8160, 2011

water circulation? It was recently demonstrated that mesoscale activities may provide ecological niches explaining the distribution of specific planktonic species (D'Ovidio et al., 2010) and that this scale should be taken into account in global biogeochemical budget (Lévy, 2008). Because of their relatively simple physical structure, anticyclonic eddies have been much studied and their biogeochemical role has been principally considered to be isolation of water (Chapman and Nof, 1988; Krom et al., 1992; Brenner, 1993; Benitez-Nelson and McGillicudy, 2008), leading towards higher oligotrophic conditions inside the eddies. However, their role in vertical exchanges of nutrients and organic matter linked with water circulation, despite their importance for the biological pump, are less well understood.

What is the influence of the complex relationships between organisms (What do we find when we open the living POC pool box)? A "world" exists between our over-simplified biogeochemical view of the biological pump (Fig. 1) and the real, multiple and complex relationships (predation, competition, symbiosis, commensalism, parasitism,...) which actually exist between organisms in the upper water. It is true that we need not only to better describe and understand these relationships (Biological population dynamics studies) but we also need to be able to simplify them in more simple functional schemes allowing to address central questions concerning global change and, for example, the role of the sea in carbon sequestration (Biogeochemical studies). These two approaches should be conducted simultaneously with increasing interactions for as long as we remain unable to describe fluxes at the level of individual organisms in the global "earth-ocean-atmosphere" model of the carbon cycle, i.e. for a long time yet!

It is of particular interest to apply these general questions to oligotrophic areas. Oceanic oligotrophic areas represent more than 50 % of the global ocean and about 40 % of total oceanic production (Antoine et al., 1996). However, the functioning and productivity of oligotrophic systems and particularly, the balance between production and mineralisation in these areas, is still the subject of much debate (Karl et al., 2003; Williams et al., 2004; Serret et al., 2006). Recent research has shown that these

BGD
8, 8091–8160, 2011

systems which were once thought to be biological deserts, may contribute significantlty to the total oceanic organic carbon export (Karl and Letelier, 2009; Kähler et al., 2010). It is thus important to thoroughly understand these vast ecosystems in order to be able to characterise them and to predict any modifications that may occur due to future environmental changes.

Among oligotrophic areas, the Low-P Low Chlorophyll (LPLC) areas such as the Sargasso Sea or the Mediterranean Sea (MS) are of further interest because a decrease in phosphate availability is the most probable decadal trend to occur with the onset of climate change (Moutin et al., 2008). The general trend seems to be towards an extension of LPLC areas, which reinforces our need to better understand their role in the carbon cycle.

2 The Mediterranean Sea and the oligotrophic ocean

Oligotrophic marine areas are characterized by a more or less pronounced thermal stratification of the water column, which delimits (1) a warm surface mixed layer with high light intensity but which is depleted in nutrients and (2) a sub-superficial layer with low light levels and more nutrients. Tropical areas, including large anticyclonic gyres, the Sargasso Sea and the MS, have long been considered as typical oligotrophic systems (Herbland and Voituriez, 1977). The depth at which nitrate concentration approaches zero during the stratified period is around 10 m in the Alboran area close to the Strait of Gibraltar, and can reach more than 150 m in the eastern basin of the MS (Moutin and Raimbault, 2002). This is related to hydrological conditions (higher winter convection in the western basin) and is also the result of the two major external sources of nutrients, the Rhône river input and the entry of the nutrient rich Atlantic surface waters, being located in the western part of the MS. The great nitracline depth in the Levantine basin (the easternmost basin of the eastern MS) is found elsewhere only in ultra-oligotrophic conditions, for example, in the centre of the South Pacific gyre. Figure 2 shows integrated primary production vs. depths at the top of the nitracline. In

BGD
8, 8091–8160, 2011

this figure, upwelling areas with high primary production and high nitrate concentration would be found on the y-axis, as would HNLC areas with low primary production and high surface nitrate concentration. Oligotrophic to ultraoligotrophic areas are presented from the left to the right. A natural oligotrophic gradient from the western to the eastern MS was observed during a previous cruise transect in 1996, with an eastern basin oligotrophy found to be as extreme as those observed in the most oligotrophic areas in the world (Moutin and Raimbault, 2002). On a regional scale, the MS presents the main oceanographic features of contrasting environments characteristic of the oligotrophic ocean.

A decrease in integrated primary production, in particulate carbon export and in nutrient availability towards the eastern side of the MS was observed, as was a deepening of the Deep Chlorophyll Maximum, while integrated chl-*a* remained constant (Moutin and Raimbault, 2002). Integrated primary production reached 150 mgC m^{-2} d^{-1} in the Levantine basin, a value considered as a limit for primary production rates under strong oligotrophic conditions. A large phytoplankton bloom is observed exclusively in the NW area throughout the late winter and spring (Siokou-Frangou et al., 2010). The duration and intensity of the spring bloom allow identifying areas in the MS in terms of yearly evolution of Sea Surface Chlorophyll-*a* (D'ortenzio and Ribera d'Alcala, 2009). The open sea waters from the western and eastern basins appear clearly distinct.

Phosphate concentrations are close to the analytical detection limits in oligotrophic surface waters, and because of this, phosphate turnover time (T_{PO_4}), which represents the ratio between natural concentration and uptake by planktonic species (Thingstad et al., 1993), is considered as the most reliable measurement of phosphate availability at the present time. T_{PO_4} varied between several hours in the MS and the Sargasso Sea during the stratified season and several months in the SP gyre, despite all these environments being oligotrophic. This allowed us to distinguish clearly between Low P and High P Low Chlorophyll areas: LPLC areas such as the MS or the Sargasso Sea with $T_{PO_4} \ll 50$ h in comparison to HPLC areas like the SP gyre with $T_{PO_4} \gg 50$ h in the upper surface stratified waters (Moutin et al., 2008).

BGD
8, 8091–8160, 2011

It has long been suspected that the low phosphate availability in the MS exerts a major control on ecosystems and carbon fluxes. Bioassays have shown that phosphate enrichment stimulates photosynthesis (Berland et al., 1980; Diaz et al., 2001). However, not only primary production, but also heterotrophic bacterial production may be controlled by phosphate availability. It has been demonstrated that phosphate limitation on bacterial production, as observed in several locations (Thingstad 1998; Zohary and Robarts, 1998), is a general feature of the western and eastern MS (Sala et al., 2002; Van Wambeke et al., 2002). Dissolved inorganic phosphate concentrations in the upper photic zone have been shown to decrease from west to east reaching levels well below 1 nM (Moutin et al., 2002). *Synechococcus* spp., the most abundant phytoplankton in surface waters of the MS during summer (Vaulot et al., 1996), have been shown to have specific advantages concerning dissolved inorganic phosphate uptake, which may explain their abundance in P depleted environments (Moutin et al., 2002). Adaptation to P limitation has also been demonstrated among higher trophic levels (Christaki et al., 1999; Dolan et al., 2002). Recent work has shown an increase in copepod egg abundance following phosphate addition to surface waters in the eastern MS (CYCLOPS), implying that copepods may be coupled to lower trophic levels through interactions which are not usually taken into account (Thingstad et al., 2005). These mechanisms are not fundamentally new, however, very few studies have dealt specifically with the consequences on the oceanic carbon cycle of possible short cuts between primary production and the export of carbon.

Nutrient limitation of organic production has been widely studied in the MS and although there is consensus as to the major control exerted by phosphate availability, nitrogen is also scarce, and the availability of silicic acid may play a central role in controlling the export of production (Leblanc et al., 2003). Biological diversity may reflect multiple organic production limitations, thus a multi-element approach is necessary to increase our understanding of marine food webs.

BGD
8, 8091–8160, 2011

Abundant evidence exists for the uncoupling between nitrogen and phosphate cycles in the MS: (1) the Nitrate:Phosphate ratio is higher in the deep Mediterranean waters than in other oceans, from 22 in the western basin (Coste et al., 1984) to 29 in the eastern Levantine basin (Krom et al., 1991), (2) the highest Nitrate:Phosphate ratios, which exceed the Redfield ratio, are found in the sub-surface waters of both the western (Mc Gill, 1961, 1965; Raimbault and Coste, 1990) and the eastern Mediterranean (Krom et al., 1991; Moutin and Raimbault, 2002) and (3), the high N:P ratios in the particulate fraction (Krom et al., 2005a). Some of these specific features of the MS as compared to the global ocean have also been observed in the Sargasso Sea (Lomas et al., 2010). At present, there is no definitive explanation for the uncoupling between nitrogen and phosphate cycles in the MS. Several hypotheses have been proposed to explain the high nitrate vs. phosphate ratio of the MS. As far as deep water is concerned, nutrient exchanges at the Strait of Gibraltar and at the Strait of Sicily, in combination with the large vertical variation of nutrient concentrations, appear as key factors in the understanding of the nutrient budget of the MS (Moutin et al., 2002). The ultraoligotrophic status of the eastern MS is principally a result of its unusual anti-estuarine circulation, in which nutrients are net exported from the eastern basin at the Strait of Sicily within the Levantine Intermediate Water (Krom et al., 2005b). The influence of these exchanges at the Straits relative to that of nutrient input from rivers has been widely discussed, with values ranging from about 10 % (Coste et al., 1988) to about 90 % (Bethoux et al., 1988) being proposed. The large P deficiency in the external input, both riverine (Ludwig et al., 2009) and atmospheric (Guerzoni et al., 1999), combined with the exchanges at the Strait of Sicily, has been hypothesized to explain the P deficiency in the eastern basin (Krom et al., 2010). Apart from hydrological fluxes, two fundementally different "internal" processes have been proposed to explain the typical NO_3:PO_4 ratios observed in deep waters. Firstly, the biological process of dinitrogen (N_2) fixation (Bethoux and Copin-Montegut, 1986; Bonin et al., 1989; Sachs and Repeta, 1999, Kerhervé et al., 2001; Pantoja et al., 2002) which may lead to nitrogen accumulation in deep waters, and secondly, chemical processes such as phosphate

BGD
8, 8091–8160, 2011

adsorption onto iron rich particles, which lead to further P depletion in the MS (Krom et al., 1991). Phosphate removal by adsorption from the water column has not been found to represent a significant sink for phosphate in the MS (Herut et al., 1999; Ridame et al., 2003), thus, N_2 fixation appears to be the key factor in explaining the high NO_3:PO_4 ratios. Nevertheless, very few measurements are available. N_2 fixation rates have recently been measured at the DYFAMED station in the western Mediterranean, and whilst these rates were typically low, this biological process does supply significant new nitrogen which may balance the nitrogen biogeochemical budget and thus explain the high nitrate/phosphate ratio in deep waters (Garcia et al., 2006). Indeed, the role of N_2 fixation in the marine nitrogen cycle has undergone increasing scrutiny and re-evaluation over the last decade, leading to increased estimates of its role in supporting oceanic new production (Karl et al., 2002). The discovery of marine diazotrophs, in addition to *Trichodesmium* spp. (Zehr et al., 2001; Montoya et al., 2004), has given a new dimension to the significance of N_2 fixation in the ocean. If significant amounts of new nitrogen are, indeed, introduced by small organisms previously thought to recycle nitrogen, our conception of the functioning of oligotrophic systems needs to be revised (Garcia et al., 2006). δ^5N data from fossilised chlorophyll (MINOS cruise) provides geochemical evidence for extensive N_2 fixation in the eastern Mediterranean (Sachs and Repeta, 1999). It has thus become of great interest to describe and quantify nitrogen input by N_2 fixation as well as to better understand the organisms responsible for this biogeochemical function.

The quantity of dissolved atmospheric N_2 is inexhaustible, so it is important to understand the control of N_2 fixation. It seems that phosphate or iron availabilities are key factors controlling these fluxes on a global ocean scale (Falkowski 1997, Karl et al., 2002). If nitrogen input by N_2 fixation is important in the MS, where low phosphate availability is thought to be the key factor controlling this flux, then the control of new production, initially defined as the fraction of production associated with new nutrients (generally nitrate), should be defined starting from new phosphate (Dugdale and Goering, 1967). It is important to further our understanding of the phosphate cycle

BGD
8, 8091–8160, 2011

in surface waters, which has hitherto been little studied (Benitez-Nelson, 2000), in order to improve our knowledge of oceanic production, particularly in oligotrophic areas. The chemical element phosphorous ^{31}P exists in the water only in the form of phosphate -organic or mineral, particulate or dissolved- and is non-reducible under natural conditions. Thus, the many complex reactions of oxydoreduction found in the nitrogen cycles are not found in the phosphate cycle (Moutin, 2000), making it possible to envisage coupling with production and the establishment of a budget from a different angle.

The MS has a wide range of oligotrophic conditions suitable for studying the transformation of organic matter in marine food webs during low new nutrient availability and provides a case study for observing the links between the C, N, P, Si and Fe-cycles. Comparisons between different systems along a longitudinal gradient of trophic status provide new insights for identifying and understanding fundamental interactions between marine biogeochemistry and ecosystems.

3 Objectives of the BOUM experiment

The BOUM (Biogeochemistry from the Oligotrophic to the Ultraoligotrophic Mediterranean) experiment has one overall goal: to obtain a better representation of the interactions between planktonic organisms and the cycle of biogenic elements, considering scales from single process to the whole MS. It is organized along three main objectives:

1. To give a longitudinal description of the biogeochemistry and biological diversity of the MS during the strongest stratified period.

2. To study the production and fate of organic matter in three oligotrophic environments located at the centre of anticyclonic eddies, with particular attention to the processes which drive the divergence of the stoichiometric ratios of the biogenic elements in the organic matter found in the surrounding water and in exported materials.

BGD
8, 8091–8160, 2011

3. To obtain a satisfactory representation of the main biogeochemical fluxes (C, N, P, Si) and the dynamics of the planktonic network, both in situ and through microcosm experiments.

4 Implementation of the BOUM cruise

The BOUM cruise took place during the summer of 2008 (16 June–20 July). The 3000 km transect, surveyed using the French Research Vessel l'Atalante, stretched from the Rhône river mouth in the western part of the MS to the Eratosthenes Seamount in the eastern part (Fig. 3). Along this transect, two types of stations (Tables 1a and b) were sampled: the so-called "short duration" (SD) and "long duration" (LD) stations (centres of anticyclonic eddies).

Thirty stations (27 SD stations + one profile at each LD station) were investigated from surface to bottom. The three LD stations were investigated over four days with a CTD cast (0–500 m) every three hours and specific operations (see below) carried out between the CTD casts. The approximate locations of the LD stations were determined using previous work and satellite imagery (IR images from I. Taupier-Letage, G. Rougier and G. Zodiatis, sea colour images from E. Bosc (Fig. 3 top and middle), all images were transmitted on board) as well as the MERCATOR forecast (www.mercator-ocean.fr). The exact locations of the LD stations were determined on board (1) from a rapid survey (Fig. 3, bottom) using XBT (roughly 10 XBT T-7 type were launched each 50 min at a vessel speed of approximately 11 nmi), and (2) using thermosalinograph and ADCP data obtained from a CTD cast (0–500 m) grid of 16 stations spaced every 3 miles and centred around the presumed centre of each eddy (Fig. 3, bottom). A mooring line (equipped with two PPS5 sediment traps, current meters, specific oxygen sensors, specific high frequency temperature sensors, consult: http://www.com.univ-mrs.fr/BOUM/spip.php?article75 for an illustration) was then deployed at the centre of each eddy to start the process study. Simultaneously, a first ARGO float (Bio) was deployed (Table 2). The mooring line was recovered at the end of

BGD
8, 8091–8160, 2011

occupation of each LD station, immediately following the last CTD cast from surface to bottom. A second ARGO float (CST3) was then deployed before departure to another station (Table 2). Specific operations during the LD station occupation consisted of radiometric cast, Marine Video Profiler cast, clean pumping for trace metals sampling, profiles of turbulence measurements (Scamp), profiles of current measurements, hauls for phytoplankton and zooplankton sampling with specific nets.

5 Water masses and general biogeochemical trends

5.1 Theta-S diagramme

The main Mediterranean water masses encountered along the BOUM cruise-transect are identified in Fig. 4. Deep waters reach an excess of potential density (σ_θ) close to 29.20 in the eastern MS and 29.12 in the western MS. A zoom of the graph for salinity and temperature of deep waters (not shown) indicates that new deep waters, since the EMT (Roether et al., 1996) were observed both in the eastern and western basins forming a scorpion tail, as already defined by Lacombe and Tchernia (1972) and Lacombe et al. (1985), bringing the lower extremities of the TS diagrams towards more dense and warmer waters.

Ascending through the water column, Mediterranean mode waters (large volumes of water formed during winter) are encountered. The "straight lines" represent the mixing between eastern deep waters and intermediate waters of Levantine origin which are normally considered to be formed to the South East of Rhodes Island, inside the cyclonic gyre near 35.5° N–28° E (Lacombe and Tchernia, 1972; Lascaraetos et al., 1993). At the eastern LD station C, the segment is long and ends with a salinity of 39.4. No decrease in salinity in the upper layers has been observed, indicating there has been no mixing with lower salinity waters. As a consequence, it can be assumed that the anticyclonic eddy C was an area of Levantine water formation during winter 2008. Older and denser Levantine waters have been identified at several stations

BGD
8, 8091–8160, 2011

between LD stations B and C. At the latter station, salinity is maximal close to the surface due to the high levels of evaporation of warm and stratified surface water at the time of the survey. This seasonal surface water is called the Levantine Surface Water and its salinity may reach 39.8, as measured in September 2008 by ARGO Float (WMO 690079). For the other stations, where no formation of intermediate water occurred during winter 2008, there is a deep salinity maximum at a depth between 400–500 m. This corresponds to the Levantine Intermediate Water (LIW) which flows out of the western basin. When approaching surface waters, the diagrams illustrate an "elbow" and finish with an almost vertical branch. This elbow corresponds to the TS properties of the previous winter's cold water at each station. By joining all these elbows with a virtual horizontal line, we find in the uppermost limit of the influence of the Levantine water. The segment (elbow-Levantine water) corresponds to the mixing of winter surface water de-salinated by water of Atlantic origin and Levantine water. Because the anticyclonic eddy C was an area of Levantine water formed during winter 2008, no signature of mixing with low salinity waters was observed in the summer profile. The salinity of the eddy C elbow is 39.4, markedly higher than the value of 39.2 measured in 2002 during the lagrangian CYCLOPS experiment (Krom et al., 2005a).

5.2 Main characteristics of the stations

The date, location and general biogeochemical characteristics of the stations investigated along the BOUM transect are presented in Tables 1a and b.

Three mixed layer depths ($MLD_{0.03}$, MLD_{2d}, W-MLD) were obtained (Table 1a) from the same vertical density profile, $\rho(z)$ at time t_p, having a 1 dbar resolution. $MLD_{0.03}$ was calculated considering the standard criterion of depth where density equals surface density $+0.03\,kg\,m^{-3}$. The two other mixed layer depths were predictions of the deeper mixed layer depths estimated between a previous initial time t_i and t_p; $t_i = 3$ days (MLD_{2d}) or $t_i = 200$ days (W-MLD) before the time t_p of the density profile measurement (see Supplement). The three ML depths were calculated from the first cast at each SD station and from the last CTD cast at each LD station, A, B and C. W-MLD

BGD
8, 8091–8160, 2011

corresponds to the maximum mixing depth that would have been measured during winter 2008, before the summer 2008 BOUM cruise. As shown in Fig. 1, the W-MLD is a fundamental variable for the estimation of biogeochemical budget and the efficiency of the biological pump. The W-MLDs were greater inside the anticyclonic eddies than outside (Table 1a). W-MLD at the LD station C in the most eastern study area of the MS reaches 400 m, or more than twice as deep as the 150 m W-MLD estimated in the nearest SD station outside the eddy. MLD_{2d} indicates the maximum mixing depth that would have been measured in a lag time of three days before the sampling. Indeed, MLD_{2d} values were similar to the maximum $MLD_{0.03}$ values measured every three hours during LD station occupation (data not shown). This is the more appropriate MLD to take into consideration for biological and biogeochemical processes occurring with time scales of orders of magnitude ranging from a few hours to several days. After omission of the very coastal SD station 27, MLD_{2d} varied between 7.5 and 29.5 m during the BOUM cruise. The EZD estimated from the discrete measurements of chl-*a* varied between 53 and 120 m, with the deeper depths being obtained in the eastern MS in accordance with the eastwardly increasing oligotrophy. Discrepancies between estimated and measured values inside the eddies (last but one and last columns of Table 1a) can be explained to a greater extent by the discrete sampling which was not always perfectly conducted to catch the chl-*a* biomass, and which thus allows an estimation at ±10 m of the EZD level.

Table 1b presents other general biogeochemical characteristics of the stations investigated along the BOUM transect.

The DCM depth increased from 40 to 140 m at a maximum value in the eastern MS, associated with the increasing trend in oligotrophy. The DCM concentrations decreased from 1.7 mg m^{-3} on the western part of the transect to 0.32 mg m^{-3} on the eastern part. A lower value of 0.15 mg m^{-3} was observed at LD station B in the centre of the Ionian basin (between the western and Levantine basins) at 75 m depth, but with a secondary maximum of 0.26 mg m^{-3} also observed deeper at 140 m. Two distinct peaks separated by at least 30 m depth were also observed in the two closest

BGD
8, 8091–8160, 2011

SD stations. After omission of the stations in the Sicilian Channel, integrated chl-*a* varied between 38.8 mg m^{-2} in the western basin and 15.5 mg m^{-2} at SD 10 in the eastern basin. An integrated chl-*a* value as low as 22.7 mg m^{-2} was measured in the western basin while a value as high as 32.6 mg m^{-2} was measured in the eastern sector. This value remains somewhat constant, as already observed by Moutin and Raimbault (2002). This observation is reinforced by the fact that part of the chl-*a* biomass is not taken into account in the eastern sector because integration was done between surface and 150 m depth only. Nutrients integration performed at the same depths gives a clear decreasing trend from the West to the East, with the exception of the value obtained at LD station A (49.0 mmol m^{-2}), which is very low when compared to the values at the surrounding stations. Mean integrated nitrate concentration was 382 mmol m^{-2} (SD = 229) in the western basin (stations 19 to 27), and 63 mmol m^{-2} (SD = 49) in the eastern basin (stations 1 to 16). The linear regression I NO_3 = 26.75* I PO_4 (r^2 = 0.90, N = 30) indicates the strong relationship between these two nutrients and a similar decreasing pattern from the West to the East. When a significant linear relationship was obtained between nitrate or phosphate concentration plotted against depth at the depths of the nutricline (related to nutrient consumption, i.e. globally related to the EZD), the slope and y-intercept of this relationship were calculated (Table 1b). The slopes enable the calculation of upward diffusive fluxes of nutrients (Bonnet et al., 2011) that will be used in the "budget", Sect. 6. As explained in Sect. 2 and shown in Fig. 1, the depth D_{NO_3} where nitrate reaches zero (y-intercept) may be considered as the best criterion for defining oligotrophy. D_{NO_3} decreases from around 50–70 m in the western basin with lower values close to 20 m near the mouth of the Rhone river, to around 80–100 m in the eastern basin with a deeper value of 114 m at LD station B. This confirms the trend from oligotrophy towards ultraoligotrophy from the West to the East in the MS. No large differences were observed between D_{NO_3} and D_{PO_4} in the eastern MS (Table 1b), contrary to other estimations based on different calculations (Pujo-Pay et al., 2011). The presence of a phosphacline close to the EZD cannot be confirmed by direct measurement due to the lack of precision of chemical

BGD
8, 8091–8160, 2011

measurements. However, the large increase in PO_4 turnover time (T_{PO_4}, one but last and last columns of Table 1b) is probably related to a "large" increase in phosphate concentration (factor 10). The PO_4 turnover time (see Moutin et al., 2002 for a detailed description of the methodology) represents the ratio between PO_4 concentration and PO_4 uptake rate by the microbial assemblage (Thingstad et al., 1993). T_{PO_4} is also the time it would take for all ambient PO_4 to be taken up, assuming no additional input (Ammerman et al., 2003). Taking into account the fact that T_{PO_4} measurement is independent of PO_4 concentration, Moutin et al. (2002) proposed an indirect method to measure it, and PO_4 concentration at nanomolar to subnanomolar levels was estimated in the surface waters of the MS. It does not seem possible to obtain a T_{PO_4} of 234 days (SD = 61) with a PO_4 concentration of around 120 nM, as was measured in the South Pacific gyre (Moutin et al., 2008) and a T_{PO_4} of several hours, as was measured in the upper surface of the MS during the BOUM cruise (Mauriac et al., 2011b), without considering nanomolar to subnanomolar levels of PO_4 concentration in the upper MS. An increase towards PO_4 concentration near the EZD of 10 nM below the detection limit of chemical measurements may represent a large increase in concentration (factor 10). Thus, it is yet not possible to draw conclusions concerning the discrepancies between nitracline and phosphacline in the eastern basin. Consequently, this argument to sustain a higher P limitation in the eastern MS should be considered with caution, as has already been recommended by Krom et al. (2005b), who found similar levels of nutricline using nanomolar methods. At some stations, a secondary nitracline was observed below the EZD, and should be related to hydrological processes and previous winter mixing rather than nutrient consumption. In these cases, a corresponding phosphacline was also observed at the same depths.

5.3 Sections

Salinity, potential temperature, oxygen concentration and apparent utilization (solubility algorithm from Benson and Krause, 1994) are presented in Fig. 5 from the Rhône river mouth in the western sector of the MS to the Eratosthenes Seamount in the eastern

BGD
8, 8091–8160, 2011

sector. The deeper waters in the western and the eastern basins are separated by the Sicily Strait (X axis at around 1100 km). The black crosses on vertical sections indicate the CTD cast position. The X-coordinate for LD stations A, B, C are approximately 450, 1750 and 3300 km, respectively, from the station in the Rhone river mouth. LD station C in the most eastern sector was above the Eratosthenes Seamount at a depth of 900 m. Specific isopycnals (σ_Θ) are drawn in thick white: 29.09 and 29.11, 29.17 and 29.19 for the western and eastern basins, respectively.

Surface temperature was 24 °C at LD station A, reaching a maximum value of 27 °C in the eastern MS. The 29.17 isopycnal in the eastern MS, at around 900 m depth, is characterized by a deep minimum in oxygen concentration and a maximum in Apparent Oxygen Utilization (AOU). Such characteristics were observed along the 29.09 isopycnal in the western MS at around 400 m depth. The fact that density layers do not correspond to oxygen layers was used by Pujo-Pay et al. (2011) in their proposal of a new way to separate different levels against depth in the MS, permitting the study of the chemical fate of organic matter. LIW formed in the eastern MS is characterized by a maximum in salinity. Leaving the influence of the anticyclonic eddies aside, LIW located around 400 m in the Ionian basin reaches the surface in the Levantine area and is not characterized there by a minimum in oxygen and a maximum in AOU. On the contrary, the layer with a maximum in AOU corresponds to the layer of LIW flowing into the western MS through the Sicilian Channel. This is because LIW is closer to the surface in the eastern MS and not completely isolated from the influence of atmospheric oxygen.

The deep minima in temperature and salinity in the more eastern part of the MS correspond to the previous Eastern Mediterranean Deep Water (pEMDW) which formed before the Eastern Mediterranean Transient (EMT), and which was observable only in the Levantine basin at around 1000 m depth (Fig. 5). The tEMDW (transient Eastern Mediterranean Deep Water) originating from the EMT is still observable in the Levantine basin (maximum in salinity around 2000 m depth, maximum in potential temperature, low oxygen concentration and higher AOU) but can no longer be seen in the

BGD
8, 8091–8160, 2011

Ionian basin. It has been replaced by a less saline, colder and with a higher oxygen content more recent deep water probably originating from the North Ionian or the Adriatic areas.

The anticyclonic eddies are easily identified by a deepening of isotherms as a consequence of deep warm anomalies, and by a deepening of isopycnals (Fig. 5). At X = 2500 km, the transect crossed the Ierapetra anticyclonic eddy to the south of Crete. At the eastern Mediterranean end of the transect, temperature at depths >1500 m was higher than at depths around 1000 m and the same feature was observed for salinity. Such a feature signals the change of deep water in the eastern MS after the EMT (1990–1991). This anomaly is easily observed on an extended TS diagram (not shown). It is noteworthy that such an anomaly was not found beneath eddy B. Anticyclonic eddies, Ierapetra included (X = 2500 km), are characterized by low AOU values (<20 µmol kg^{-1}) close to the surface and even deeper down to 200 m, particularly at LD station C (Fig. 5). At LD station B, AOU was also low near 500 m, but was not as low as at LD station C. This indicates the presence of recent Levantine waters. Deeper yet and down to the bottom, AOU was higher, indicating that recent deep waters with an AOU close to 60 µmol kg^{-1} do not penetrate this eddy, which has an influence on the whole water column. This could indicate that it is an old eddy. Eddy A did not have a deep, strong signature for salinity and AOU (Fig. 5).

Nutrients concentrations (Fig. 6) are close to zero in the upper surface and decrease from the West to the East in accordance with classical trends in the MS. A detailed description is given by Pujo-Pay et al. (2011). In this figure, the scales for nitrate and phosphate follow the Rr (Rr = Redfield ratio). Because the colours are not identical for nitrate and phosphate, the strong depletion in P vs. N in the whole MS, which is even higher in the eastern part, can be clearly seen. Maxima of nitrate and phosphate concentrations occurred within the intermediate depths between 500 and 1000 m. These maxima are closely related and correspond to the maxima of organic matter remineralisation. The three eddies studied, A, B, C, as well the other eddies crossed during the transect, are easily observable in T, S (Fig. 5) and are also visible in nutrients

BGD
8, 8091–8160, 2011

concentrations (Fig. 6). The variable P^* (Deutsch et al., 2007) was calculated as $P^* = PO_4 – NO_3/Rr$ and plotted in Fig. 6. P^* values were close to zero in surface waters reaching 0.1 µM at a maximum value but because PO_4 measurements are very close to the detection limit in surface waters, these results should be taken with caution. Negative P^* values were measured in deep waters confirming the P deficiency of Mediterranean waters and the very particular oligotrophy of these waters compared to other oligotrophic areas in the world ocean, such as the South Pacific gyre which is considered as the most oligotrophic area of the ocean (Claustre and Maritorena, 2003) and where P^* never reaches negative values (Moutin et al., 2008). Negative P^* values of −0.119 µM (SD = 0.014 µM) were observed both in the eastern and the western deep Mediterranean waters, indicating that the relative variations of nitrate and phosphate concentrations in deep waters occurred in a proportion that conserves P^*, i.e. with a constant and low variable NO3:PO_4 ratio. A Rr of 17.7 below 250 m was considered as suggested by Pujo-Pay et al. (2011). The most probable explanation for this result is that mineralisation of organic matter in deep waters follows the Rr and that the deep exported material has probably relative N and P concentrations close to the Rr, as previously hypothesized by Redfield et al. (1963). As diatoms and their predators are known to better follow the Rr ratio than smaller organisms, and because they might play an unexpected role even in the very oligotrophic waters of the MS (Crombet et al., 2011; Nowaczyck et al., 2011), their relative contributions to the carbon cycle and export need to be reconsidered. A decrease in P^* towards a water parcel could be associated with N_2 fixation (Deutsch et al., 2007). Such a feature is not shown in Fig. 6 even in the intermediate waters known to flow from the eastern to the western MS waters. This could be related to the relatively low N_2 fixation rates measured (Krom et al., 2010; Bonnet et al., 2011), even if the presence of diazotrophic organisms in the MS is no longer questionable (Le-Moal et al., 2011).

"Chlorophyll" concentration (in situ Fluorescence Units) illustrated the deepening of the Deep Chlorophyll Maximum (DCM) from West to East (Fig. 7). This is associated with the increasing trend in oligotrophy and is shown as the deepening of the top of the

BGD
8, 8091–8160, 2011

nitracline (Table 1b, see also Fig. 2). The strong relationship between the top of the nitracline and the DCM has already been described (Herbland and Voituriez, 1979), and is directly related to the winter mixed layer depths (Table 1a) with the exception of inside the eddies and in the NW MS. The DCM may correspond to an equilibrium depth where new biomass is maintained by diffusion of new nitrate from below. Diffusion fluxes are very low during the BOUM cruise stratified period (Cuypers et al., 2011) and the DCM should rather be seen to result from nitrate exhaustion of surface water by biological uptake and export at the time of the measurements. It is also probable that the biomass at the DCM is primarily fuelled by regeneration of nutrients, as it is in the upper surface (Moutin et al., 2002). It is not possible to exhaust the nitrate deeper than the euphotic zone (Table 1a) because it is directly linked to photosynthesis. Thus, the DCM depth, the euphotic layer depth and the top of the nitracline depth are clearly correlated, and deepen from the West to the East of the MS. This is not the case in the NW MS and nor inside the eddies because the previous winter mixing in these areas is deeper than the depth of the layer that is subjected to nitrate depletion during the stratified period. A first level of interpretation suggests that anticyclonic eddies may bring nutrients up to the surface from deeper water, allowing higher production and subsequently increasing the biological pump. Nevertheless, because of the deepening of the isohalines and the isonitrate concentrations, the net input of nitrate in the photic zone is expected to be virtually the same as outside the eddies, and so the biological pump is not changed. In any case, it is not possible to draw a conclusive picture of the real role of anticyclonic eddies on the biological pump without taking into account the possible lateral exchanges of waters and the fate of the eddies. As a very first approximation in this paper, we will consider that these eddies are in solid body rotation and are closed systems similar to giant mesocosms for biological and biogeochemical process studies.

The more detailed scale of depth (0–500 dbar) in Fig. 7 as compared to Fig. 5 enables to locate the LIW. During winter, LIW (S = 39.4) was located at the surface in the Levantine basin and reached an anomalous Salinity of 39.7 inside the Cyprus eddy

BGD
8, 8091–8160, 2011

(LD C) which is a source of LIW. LIW is located close to 150 dbar from the eastern Levantine basin to the Ionian basin where it deepens to 400 dbar before reaching the Sicilian Channel. The eddies are clearly marked by a deepening of the isohalines. AOU (Fig. 7) is slightly negative in the mixed layer (around 15 m depth, see Table 1a) which corresponds to a slight O_2 oversaturation of 6–10 µmol kg^{-1}, as is classically observed in upper marine waters. AOU reaches −20 µmol kg^{-1} below the pycnocline (around 15–30 m) under the influence of the spring net community production which occurs after the stratification of the water column (strong deceleration of oxygen transfer) and the heating by penetrating solar radiation which accounts for a solubility decrease of 10–15 µmol kg^{-1} in July in the MS. AOU reaches positive values at approximately the depth of the DCM. This latter depth also corresponds approximately to the W-MLD (Table 1a) and to the depth at the top of the nitracline, except in areas of strong deep water formation (NW MS and eddy C). The fact that W-MLD corresponds to a depth where AOU is nil (Fig. 7) indicates that lower depths are ventilated during winter with a positive net community production when stratification occurs, whereas deeper depths show AOU>0, indicating more mineralisation than production (negative net community production) for the same period of time (between winter and summer).

5.4 Main characteristics of the three anticyclonic eddies (A, B, and C)

As shown in Fig. 8a, on board measurements of the mean ADCP currents, taken along the ship's transect at depths between 29 and 125 m, indicate that the three sites were at the centres of anticyclonic eddies. Figure 8a (bottom) provides evidence that locations of the LD stations were near the axis (<10 km) of the eddies, but drifted with the drift of the centres. The positioning at the centres of anticyclonic eddies is confirmed by the particular variations of several variables along the BOUM transect shown in Fig. 8b. The three upper panels represent differences between depth-averaged values (20–850 dbar) and the mean values for the whole transect for AOU (µmol kg^{-1}), Salinity and excess density (kg m^{-3}) along the BOUM transect. The bottom panel shows the variations of the flux function F calculated for each cast by the integration of the geopotential

BGD
8, 8091–8160, 2011

anomaly referenced at 850 dbar. This function F is very useful because the difference between 2 points, whatever their distance apart, is exactly equal to the baroclinic geostrophic transport with a sign directed positively and perpendicularly at the transect on the right. As an example, for eddy B (cast 115, X = 1808 km), $F = -28.437$ Sv and for the next cast on the transect (cast 2, X = 1939 km), $F = -31.880$, thus $\delta F = -28.437 + 31.880 = 3.443$ Sv. Each peak of the function $F(X)$ indicates the presence of an anticyclonic eddy between 2 adjacent stations, or possibly the presence of meanders, but this should be disregarded when considering surface ADCP currents (Fig. 8).

The variables (Fig. 8b) show trends indicating general features of the MS and distinctive spikes indicating the presence of eddies. Salinity increased towards the East and reached its maximum value in the Levantine basin. Overall sea level decreased (Fig. 8) due to waters below 200 dbar being denser and saltier in the eastern basin than they are in the western basin. It is less well-known that AOU is lower in the East than in the West for the same water level, yet this is not very surprising when the general gradient in organic matter production towards the East (Moutin and Raimbault, 2002) is considered. The positions of the LD stations A, B, and C are marked by an increase in F(X) and a decrease in AOU and in excess density, as expected for anticyclonic eddies. However, at LD station A, a decrease in Salinity is observed while an increase is seen at LD stations B and C: this will be explained later when considering water masses and the structure of each eddy. The transect also crossed eddies which had not been chosen for process study such as the Ierapetra anticyclonic eddy (Fusco et al., 2003) to the south east of Crete (X≈2450 km) with its strong AOU anomaly, and the more easterly (X≈2800 km) Mersa-Matruh eddy (Robinson et al., 1991). An increase in Dissolved Organic Carbon (DOC) was observed inside each eddy we crossed (Fig. 8b). This was generally associated with a decrease in Dissolved Inorganic Carbon (DIC) except in the case of eddy C.

Analysis of the drifting of the mooring lines and of the float trajectories (not shown) indicates that the R/V was located at less than three km from the centres of the eddy at

BGD
8, 8091–8160, 2011

the beginning of the LD stations. Their diameters were close to 100 km and the studied areas were under 10 km from the centre of the eddies.

The main physical, chemical and dynamical characteristics of the three studied eddies are synthesized in Fig. 9 (middle) and Table 3. Figure 9 shows the superimposed vertical profiles of two casts for each eddy, one cast very close to the eddy axis (<10 km from axis, casts 186, 114 and 71 for LD stations A, B and C, respectively) which is later called "in" profile and one cast outside the eddy (>70 km from axis, casts 130, 2 and 17 for SD stations 22, 1 and 11, respectively) which is later called "out" profile. The location of each chosen cast is indicated on Fig. 3 with red dots. Comparison between these pairs of casts has already been used to evidence the existence of eddies (Fig. 8b). Figure 9 (top) shows the vertical profiles of T, S and AOU, those of the anomalies as defined below (Middle) and those of primary production, chl-*a*, σ_θ, NO_3 (middle bottom).

Table 3 presents specific characteristics of the three studied eddies. It concerns (1) general properties obtained from direct observations, (2) anomalies determined from the two "in" and "out" casts for each eddy, and (3) dynamical properties calculated from observations of a vessel-mounted ADCP (see Supplement including a comparison between the observations and the simulated eddy A). These specific characteristics are defined only in the legend of Table 3.

Before presenting the specific characteristics of the eddies, it is useful to briefly recall the dynamical specificity of mesoscale anticyclonic eddies. A surface intensified mesoscale eddy in an ocean in rotation (f >0 in the Northern Hemisphere) shows the following dynamical properties (Defant, 1961): Geopotential differences "in" – "out" (δG(z)) is >0, azimuthal velocity (Vaz) is <0 at any depth, and the transport function (T) between the two casts is locally maximum. These specific characteristics are observed for the three studied eddies (Table 3 and Fig. 8b).

The isopycnal lines deepen (see ΔH, Table 3) towards the eddy centre, at least when Vaz is decreasing with depth. When Vaz is increasing with decreasing depth, the isopycnal slope is reversed (see Fig. 4 in McGilliccudy et al., 1999, mode water eddy

BGD
8, 8091–8160, 2011

case), as was observed close to the surface in our eddies. In this case, the maximal absolute velocity Vaz_{Max} occurs not at surface but at a depth $DVaz_{Max}$ below the surface and at a horizontal distance $rVaz_{Max}$ from the eddy axis.

Due to the deepening of the isopycnal lines, the vertical spacing of isopycnals increases and the square of the Brunt Vaïssala frequency ($N^2 = -g/\rho.\partial\sigma/\partial z$) decreases near to the axis. Hence, a pycnostad appears on the "in" profile. At depths greater than the depth of maximum σ anomaly, N^2 for the "in" profile is higher than for the "out" profile because at great depths, density is the same for both profiles.

In addition, as the relative vorticity ζ calculated as $2\omega/f$ is negative near the axis for an anticyclonic eddy, the absolute potential vorticity near the axis is $f\ N^2/g(1+\zeta/f)$ and less than the same for "out" profile. It is due firstly to N^2 and secondly to the negative value of ζ. Thus, the inner part of an eddy is characterized by a trough of absolute potential vorticity which isolates the eddy core in solid rotation from any outer advection. The horizontal limits of this trough are given in Supplement. When the eddy rotation velocity is sufficiently high, a pycnostad with a nil vertical gradient occurs when $|\zeta| = f$. This may happen during eddy formation, particularly in winter (Krom et al., 1992). However, in spring and summer, the top of the eddy is warmed and some geostrophic adjustments occur. As a consequence, the vertical density gradient is not nil but has a lower value than outside the eddy (Chapman and Nof, 1988) and the eddy takes the shape of a mode water eddy (Pingree and Le Cann, 1992; McGilliccudy et al., 1999). Below the warmed part of the eddy, horizontal anomalies, as described hereafter, are conserved. Thus, the so-called anomalies are typical properties of each eddy and are easy to observe from CTD casts. They provide information about the period and location of the eddy formation. It is interesting to note (Table 3) that inferred ζ, <0, remains a sizeable fraction of f, roughly -0.3 to $-0.4f$, and is the same order of magnitude as that observed for meddies, smeddies or swoddies (Pingree and Le Cann, 1992, 1993).

Horizontal anomalies are conserved inside the body of water around the axis because it is isolated from mixing and advection form surrounding waters during life time

BGD
8, 8091–8160, 2011

of the eddy. This is due to the strong influence of ζ on potential vorticity conservation (see Supplement treating the shape of such a body of water). As a consequence, the winter time mixed layer depth is greater "in" than at the corresponding "out" station and the body water's are more recent and more oxygenated inside the eddy. This is the reason why an anomaly of AOU corresponds to anomalies in σ, potential temperature (θ) and S.

Table 3 reports the extreme values observed as δ differences between "in" and "out" casts for σ, θ, S and AOU and Fig. 9 (middle) shows the depth profiles of each anomaly and of the geopotential (δG). The maximum anomalies are also indicated and noted, for example $\sigma^{E}_{\mathrm{MaxAno}}$, without taking into account the real sign of the anomaly which is <0 for σ, θ, AOU and >0 or <0 for S. The depths of observed maximum anomalies are also indicated in Table 3 using the depths of maximum density anomalies, without taking into account the possible deviations to real depths for each parameter. These changes are in any case weak (Fig. 9, middle). Higher anomalies appeared on S and AOU, but they are also significant on θ and σ.

θS properties of anomalies are indicated as red dots on Fig. 4 for the depth range between the top and the maximum of anomalies. This shows that the depth ranges of significant anomalies are in the non warmed part of the θS diagrams (Fig. 4) but not far beneath this. Maximum anomalies correspond to the densest waters and the lower extremities. These extremities are close (at least for $\mathrm{B_{deep}}$ and C) to the θS properties of the "out" station but with a difference in depth of ΔH m. These anomalies are on the representative LIW line for C and $\mathrm{B_{deep}}$ eddies, and are in the range of winter Modified Atlantic Water (MAW) θS properties for A and $\mathrm{B_{surf}}$ eddies. These are indications that all three eddies were formed during the winter period.

Anomalies also help to locate the eddies during the winter of their formation. Eddy C was probably formed at the same location it occupied during summer 2008 because at the maximum anomaly depth, θS properties correspond to the saltiest and warmest limits known for LIW (Fig. 4). However, the characteristics of the anomalies for $\mathrm{B_{deep}}$ cannot correspond to the winter 2008 location, where estimated W-MLD reached only

BGD
8, 8091–8160, 2011

109 m (Table 3), or about 200 m above the observed depth range of the B_{deep} anomaly. Indeed, θS characteristics at $D^{E_{MaxAno}}$ indicate that formation may have occurred in the northern part of the Ionian Sea, near the eastern Greek coast (Pelops area). The deep eddy B was formed a winter before 2008, as confirmed by low $AOU^{E_{MaxAno}}$ values, which indicate recent ventilation. The strong δAOU^{E} observed in summer 2008 is consistent with a drifting of the eddy since its formation south westwards in an area where the age of water is older at $D^{E_{MaxAno}}$. A 400 km drift probably took more than a year, its exact duration cannot be estimated at present. Eddy B_{surf} formed with MAW, and δAOU^{E} is consistent with a formation, or at least a ventilation, during winter 2008 considering W-MLD 2008. Such trapping of surface outer water by an eddy, and intensification of the dynamic properties of an existing deep eddy, cannot be discussed here, but it is probably linked to interaction between the eddy and MAW jet. Eddy A is clearly formed with MAW generally observed in the Algerian basin and possibly during winter 2008, considering the low AOU at depth and θS properties of anomalies. This eddy is the least deep of the three studied.

One main concern for biological and biogeochemical studies and budgets is to know if eddies can be considered as closed systems dating back to the previous winter, in particular close to the surface. If anomalies in the 0–100 m range are weak, the main dynamical properties (relative vorticity, geopotential, see δG, Fig. 9 middle) are still different from the outer part of the eddies and a potential vorticity barrier up to the warmed surface subsists. As already observed by Chapman and Nof (1988), this vorticity barrier prevents any strong mixing and advection of outer water inside the eddy and explains why the depth range of eddies starts from the surface (Table 3).

The cores of each eddy were found at depth (Table 3) where large differences between "in" and "out" casts for S and AOU were observed (Fig. 9 top). At the centre of each eddy, a distinct pycnostad was observed which showed very little salinity change against depth (100–250, 300–600, 150–380 dbar for LD stations A, B, C, respectively). Nevertheless, a slight stratification remains inside the cores of the eddies, as is shown by the non-zero T and S vertical gradients. However, for the same depths, AOU is

BGD
8, 8091–8160, 2011

constant (C), slightly decreasing (B) or slightly increasing (A) while a regular and more classical AOU increase outside the eddies was observed (Fig. 9 top). Below the deeper depth of the core, stratification (vertical gradient of density) increases and the vertical gradients of the other variables are stronger than outside the eddies, so that the profiles of each variable are virtually the same below a certain depth which can be considered as the bottom of the eddy (420, 1200 and 800 m for LD stations A, B and C, respectively). The influence of the eddies could be much deeper and different depths were obtained when small dynamic anomalies were considered (Table 3) or fine scale changes in AOU (Fig. 5).

Primary production rates were higher close to the surface and decreased down to zero at, or just below, the euphotic zone depth (Fig. 9 bottom). The top of the nitracline corresponds to the DCM depth at each station. A secondary nitracline, related to the winter mixed layer (Table 1b), was observed at LD station C. As previously noted, the first nitracline is the result of biological N production and export occurring after the previous winter mixing. Although discrete sampling was relatively sparse at depth, similar profiles were observed for nitrate concentration with relatively low variations (changes in the vertical gradients) observable inside the cores of the eddies. Noteworthy identical differences between profiles from "in" and "outside" the eddies were observed for nitrate concentration and AOU. This result is probably related to remineralisation, which leads to the same ratios between oxygen consumption and nitrate production (Redfield et al., 1963). Less or even no organic matter was remineralised inside the cores of the eddies, either because of less or even no organic matter input, or because of lack of time for mineralisation (see Sect. 6). The deeper DCM (Fig. 9 bottom) and lower integrated chl-*a* concentration between 0–150 m (Table 1b), indicators of a stronger oligotrophy, are found inside the eddy B in the Ionian basin and not, as expected, in the Levantine basin of the MS. The EZD reaches 104 ± 4 m at a maximum value inside the Ionian area at LD station B. Integrated mean primary production measured in situ inside the three studied eddies, A, B and C, were 160, 190 and 164 mgC m^{-2} d^{-1} (Christaki et al., 2011), for a nitracline depth of 72, 114 and 93 m, respectively. The results confirm

BGD
8, 8091–8160, 2011

the previous conclusion that IPP about 150 mgC m^{-2} d^{-1} (obtained using 24-h in situ incubation from dusk-to-dusk, as recommended for JGOFS) may appear as a lower limit for IPP during strong oligotrophic conditions (Moutin et al., 2002). The mesoscale activity is strong enough to delete (or even reverse) the very well-known western to eastern gradient of trophic conditions in the MS.

Short-term temporal trends

LD stations A, B and C were occupied for 4 days, allowing the study of short-term variations in biogeochemical properties using CTD casts undertaken every 3 h. A total of 32, 33 and 32 casts were performed for LD stations A, B and C, respectively. Figure 10 shows the superposition of all vertical profiles vs. depth (dbar) of excess density (kg m^{-3}), potential temperature (°C), dissolved oxygen (µmol kg^{-1}), total chl-*a* (mg m^{-3}), Salinity (PSU), ISUS nitrate concentration (µM), AOU (µmol kg^{-1}) and *Cp* (m^{-1}), obtained at LD stations A, B, C. The first observation to note is the very low variability between each profile (of about 30) as is expected from stations located in the centre of anticyclonic eddies. This allows the comparison of an "in" and an "out" profile, as was described for the previous figure (Fig. 9). The properties of the cores are shown by a break on the vertical gradients in excess density, potential temperature and Salinity for specific depths (Table 3). A maximum in oxygen concentration, and corresponding minimum in AOU (which may even be negative) were observed between 40–60 m just beneath the surface thermocline while oxygen concentration in the upper surface water was near saturation (about 2 %). The slight oversaturation is linked to oxygen solubilisation following warming in the upper surface water. As indicated above, the oxygen and nitrate concentrations were remarkably constant in the core of eddy C although this was not exactly the case for density between 120 and 380 m. The same pattern was observed for the deep core of eddy B (300–600 m). The main nitracline was encountered at the base of the core of each eddy, 200, 650 and 380 m for LD stations A, B and C, respectively. The nitrate concentrations inside the

BGD
8, 8091–8160, 2011

eddies were relatively low, 1.0, 2.1 and 0.8 µM for LD stations A, B and C, respectively. A secondary nutricline was encountered at the top of the cores, reaching the upper surface waters with their classically zero nitrate concentration. Maximum Total chl-*a* concentration reached 0.92, 0.29 and 0.70 µg l^{-1} for LD stations A, B and C, respectively, with variations of concentrations reaching 30 % for the different casts. The depths of the maximum of Total chl-*a* concentrations corresponded to the 1 % of incident light level, excepted for eddy B (0.3 %). This may be related to an artefact in the conversion between fluorescence and concentration, as explained at the end of this section.

Figure 11 represents the temporal sections between 0–200 m depth of tchl-*a* (mg m^{-3}) and of the optical attenuation coefficient *Cp* (m^{-1}) for the particles. The temporal scale on the X-axis is given in 2008 Julian days and the dates of the profiles are indicated by red crosses near 170 dbar. *Cp* is obtained from *Cm* as measured with a Seapoint transmissiometer with a 25 cm optical length in seawater, by subtracting the depth-averaged value of *Cm* between 450–500 m where *Cp* is considered negligible (Loisel and Morel, 1998). On each panel, isopycnals (σ_Θ) are drawn with thin black lines at 0.1 kg m^{-3} intervals in deeper layers from 25.7, 26.2 and 26.4 for LD stations A, B and C, respectively, and with white lines at intervals of 0.03 kg m^{-3} near the surface in the range (25.21–25.39), (25.31–25.61) and (26.30–26.48) for LD stations A, B and C, respectively. The daily changes in density of the mixed layers are clearly evidenced. In addition, $MLD_{0.03}$ are plotted as red stars.

The temporal variations of tchl-*a* and *Cp* (Fig. 11) are in good agreement, indicating maxima of phytoplankton biomass and of particles at the same depths, 90, 75 and 110 dbar for LD stations A, B and C, respectively. The depths of these maxima fluctuate with the same temporal periodicity as for isopycnals, suggesting an influence of ±10 m of near inertial internal waves. The amplitude of the waves varied against depth, as is shown by the vertical oscillations of the isopycnals, and was particularly low along strong density gradients (pycnocline and thermocline) as well as inside the core of the eddies. The internal waves also have an influence on the MLD. These depths reached minimum values between 0–4 h local time during the nights, i.e. when buoyancy fluxes

BGD
8, 8091–8160, 2011

were negative (red crosses in Fig. 11).

A distinct diurnal maximum in *Cp* occurred between 12:00–16:00 h local time above the DCM. At LD station B (and nearby SD stations), a maximum of tchl-*a* was observed at 135 m depth despite there being no observable variations in *Cp*. This is probably related to divinyl chl-*a* fluorescence associated with *prochlorococcus* spp. populations, because maxima of chlo-*b* and of zeaxanthine were also observed at the same depth (data not shown). When considering the bottle measurements instead of the tchl-*a* estimated from the fluorescence, no tchl-*a* maximum was observed at 135 m depth (Fig. 9 bottom) and only one was observed at 113 m which is why this maximum should be considered as an artifact in the conversion of Fluorescence Units to tchl-*a* concentration.

6 First order biogeochemical budgets

Data obtained from sediment trap deployment are presented in Table 4. Methods are detailed on the French national "traps" web site (http://www.obs-vlfr.fr/LOV/Pieges).

Daily N-budget at the LD stations

A first order daily N-budget was carried out at the three LD stations (Table 5). N-input by eddy diffusion is the product of the eddy diffusion coefficient measured at the level of the nitracline (Cuypers et al., 2011) by the gradients of concentration S_{NO_3} (Table 1b). N-input by N_2 fixation is the mean integrated value measured in the photic zone (Bonnet et al., 2011). New N-input corresponds to the sum of these two fluxes, first because other possible inputs are neglected and second, because the eddies are presumed to be closed systems after their formation. N-export corresponds to the mean value measured on drifting traps at 230 m (Table 4) during the occupation of each site. N-primary production is determined by dividing the gross C-primary production (GPP) by 6.6, the classical C:N ratio of particulate organic matter. GPP corresponds to 1.72*NPP,

BGD
8, 8091–8160, 2011

the net primary production (NPP) measured in situ with the ^{14}C method (Moutin et al., 1999). The percentage of export production is calculated by dividing the export by the GPP. The percentage of production attributed to nutrients regeneration in the photic zone is estimated by the difference with the export production at 230 m.

Inputs by eddy diffusion and N_2 fixation are virtually identical at LD stations A and B whereas N_2 fixation is definitely weaker at the eastern LD station C. This counter intuitive result is discussed by Bonnet et al. (2011). N-input by N_2 fixation during the strongly stratified period may represent a significant part (up to 55.3 %) of new production, a percentage close to previous estimations in oligotrophic areas (Karl et al., 2002). The use of estimated eddy diffusion coefficients for the calculation of diffusive fluxes is considered as a prime source of inaccuracy (Krom et al., 1991; Moutin and Raimbault, 2002). Therefore, real measurements using high frequency temperature measurements were carried out during the BOUM cruise (Cuypers et al., 2011). Nevertheless, the mean value measured ($0.86\,m^{-2}\,j^{-1}$) is in the $0.1–2\,m^{-2}\,j^{-1}$ (i.e. $0.1–2.3\times10^{-5}\,m^{-2}\,s^{-1}$) range previously estimated by Moutin and Raimbault (2002), using the turbulent energy dissipation rate (ε) proposed by Gregg (1989) and the buoyancy frequency $N(z)$ calculated according to Osborn (1980). The new N-input in the photic zone is virtually identical to the N-export measured at 230 m by drifting traps. This means that the eddies are close to an equilibrium state where input equals loss.

The slightly higher values, particularly at LD station C, could mean that systems tend towards this equilibrium but also that little organic matter remains to be exported from the last "spring" bloom. The unexpected discovery of numerous diatoms at LD station C (Crombet et al., 2011) corroborates this assumption. During the strongest stratified period of the BOUM cruise, export represents approximately 1 % of GPP, which is therefore 99 % fueled by nutrients regenerated in the photic zone. These results are among the lowest obtained in the Mediterranean Sea and in the oligotrophic ocean in general (Moutin and Raimbault, 2002). It is important to note that mineralisation of particulate organic matter between the deepest depth where NPP was measured (around 150 m) and the first depth where traps were deployed (230 m) is not considered

BGD
8, 8091–8160, 2011

in our calculation. However, this is probably extremely low given the near identical values obtained at 230 and 460 m at LD station C (Table 4).

Annual N-budget at the LD stations

Data are presented in Table 6. The euphotic zone depth (EZD) and the winter mixed layer depth (W-MLD) were presented in Table 1a. Concentration at the W-MLD is obtained from the closest Niskin bottle (depth indicated in brackets) considering no seasonal change at this depth. Following the complete vertical mixing from surface to this depth, this concentration was the surface nitrate concentration during the previous winter, $[NO_3]_{W-ML}$. As nitrate concentration is under chemical detection limit over the greater part of the photic zone during the strongest stratified period (Fig. 9 bottom), the annual nitrate input by winter convection in 2008 is estimated using the product of $[NO_3]_{WML}$* EZD. Annual N-input by N_2 fixation is estimated at 365* daily N-input, i.e. we considered that destratification did not influence N_2 fixation, which we take as being constant over the year for reasons of simplification. Annual N-input by eddy diffusion is estimated using the product of the daily N-input* 304, i.e. we considered a stratification period of 10 months with an established stratification, as observed during the BOUM cruise, and a convection period of 2 months. Annual new N-input is considered as the sum of inputs per winter convection, eddy diffusion and N_2 fixation. The percentages of each in comparison with the global annual input are calculated together with the minimal annual export (background export) which we take as being identical to the daily export measured during the stratified period throughout the year. It is then possible to determine the percentage of export not linked to the background, i.e. export which probably occurred just after the spring bloom ("Spring" export), by its difference with the global new input and considering that the latter equal the annual export production (Eppley and Peterson, 1979).

The annual N-input during the 2008 winter convection is extremely variable inside eddies. It can be nil (eddy B) because the W-MLD did not reach the depth required for restocking of nutrients. On the other hand, it is the main source of new N for eddy

BGD
8, 8091–8160, 2011

A (83.5 %) and for eddy C (91.9 %). Inputs through eddy diffusion and N_2 fixation are virtually identical on an annual scale and are of a similar order of magnitude for eddies A and B. N_2 fixation is extremely low inside eddy C in the eastern MS, whereas it is slightly above the level of input through turbulent diffusion inside eddy A in the northern MS. The annual "background" export is approximately 10 mmol m^{-2} y^{-1} for the three eddies. Export outside of this period may represent more than 80 % of the annual export (LD stations A and C) and may also be nil (LD station B). This is in keeping with the strongest oligotrophic characteristics of eddy B and with the presence of diatoms and of a maximum of biogenic silica at LD C (Crombet et al., 2011). It is likely that spring "blooms" are probably not regularly observed from space in oligotrophic areas because they occur principally at non-observable depths (below 50 m). Thus, the distinction between "non-bloom" and "bloom" areas as evidenced by satellite imagery (D'Ortenzio and Ribera d'Alcala, 2009) may need to be questioned, as suggested by observations (Crombet et al., 2011). The previous winter mixed layer depth reached appears to be a fundamental criterion for new nutrients availability. Extreme spatial variability exists between eddies, with W-MLD from 90.5 m at LD station A to 396.5 m at LD station C. W-MLDs are always deeper inside the eddies than outside where they are in keeping with climatological means. Temporal variability may also be high, particularly on an annual basis. The previous W-MLD of eddy B is likely to be deeper than the depth reached during winter 2008.

It should be recalled that for this first order annual N-budget, new production (in the sense of Dugdale and Goering, 1967) related to winter convection (non stratified period) was calculated by considering initial stocks of biomasses to be negligible as well as the net dissolved organic production. Moreover, atmospheric deposition of dust was omitted because of its high spatial and temporal variability, even if its relative importance in the N-budget has recently been re-evaluated (Markaki et al., 2010). Finally, eddies were considered as closed systems and further budgets should take into account possible exchanges with surrounding waters.

BGD
8, 8091–8160, 2011

The input of new nutrients and particularly of new nitrogen in the photic zone is considered as the first criterion in oceanic fertility (Minas et al., 1988). Nevertheless, sequestration of anthropogenic CO_2 depends on a budget which takes greater depth into account. It is important to know what fraction of export production escapes mineralisation on a decadal time scale (Fig. 1) and is then exported to deeper depths, i.e. to know what fraction will reach deep circulation.

Towards a carbon budget

The fact that AOU was low inside the eddies, together with the near-identical export measured at 230 and 460 m, seems to indicate that eddy cores are areas where low mineralisation of particulate organic matter occurs. This can probably be related to the pycnostads observed inside the eddies in favor of a deeper settling of particles inside the eddies that outside. "In" and "out" AOU comparison (Fig. 9 top) indicates lower mineralisation inside the eddies. Assuming a similar primary production inside and outside, the anticyclonic eddies will be more efficient for anthropogenic CO_2 sequestration through sedimentation of particulate organic matter. The difference in mineralisation (Fig. 9 top) should probably be attributed primarily to the ages of water masses, which are predominantly younger inside the eddies than outside. A thorough budget should also focus on this subject.

The three eddies are enriched in dissolved organic carbon (DOC), (Fig. 8b). Sequestration of anthropogenic CO_2 by vertical export of accumulated DOC seems thus to be higher inside eddies. It is considered to be the main organic carbon transport from surface to deeper layers in the MS (Copin Montégut and Avril, 1993, Avril 2002). In addition, this sequestration seems to be accentuated by anticyclonic eddies and probably occurs primarily when the eddy disappears. The life of anticyclonic eddies in the MS varies between several months to several years (Puillat et al., 2002; Taupier-Letage, 2008). The very rapid displacement of the PROVOR float (WMO 6900679) during winter 2009 seems to indicate that eddy C disappeared just after the observation of substantial vertical mixing. LIW are formed in eddy C (Sect. 5.1) which thus

BGD
8, 8091–8160, 2011

can be deemed very efficient in trapping accumulated DOC in the intermediate water circulation. Accumulation of DOC in the upper surface waters can be attributed to various causes. Low phosphate availability renders heterotrophic bacteria more limited by phosphate than by carbon, leading to DOC accumulation (Thingstad et al., 1997). The unusually high N:P ratio of the MS which may favor the uncoupling between growth and carbon production also leads to DOC accumulation (Mauriac et al., 2011a). The relative importance of DOC transport in the biological pump is probably one of the main characteristics of LPLC areas, and it is likely reinforced inside anticyclonic eddies.

7 Special issue presentation

The goal of this special issue is to present the knowledge obtained concerning the functioning of the MS ecosystems and associated biogeochemical cycles based on the dataset acquired during the BOUM experiment. The cruise strategy was organized to promote collaborations between physicists, biogeochemists, biologists and modellers. Most of the contributions to this volume have taken advantage of this collective effort. The papers below are introduced according to the three main objectives of the BOUM experiment.

1. Longitudinal description of the biogeochemistry and biological diversity of the MS during the strongest stratified period.

   Distribution of the following parameters were studied along the East-West 3000 km BOUM transect: particulate and dissolved organic and mineral nutrients (Pujo-Pay et al., 2011; Crombet et al., 2011), phospholipids (Poppendorf et al., 2011), aerosol composition (Ternon et al., 2011), photosynthetic production of dissolved and particulate organic carbon (Lopez-Sandoval et al., 2011), planktonic N_2 fixation (Bonnet et al., 2011), species richness of unicellular and filamentous diazotrophs (Le Moal et al., 2011), diatoms (Crombet et al., 2011), dinospores and their host diversity (Siano et al., 2011), picocyanobacteria Prochlorococcus

BGD
8, 8091–8160, 2011

and Synechococcus (Mella-Flores et al., 2011), heterotrophic bacterioplankton abundance and production (Van Wambeke et al., 2011), distribution of the major members of the heterotrophic microbial food web (Christaki et al., 2011; Talarmin et al., 2011), Aerobic anoxygenic phototrophic (AAP) bacteria (Lamy et al., 2011) and their diversity (Jeanthon et al., 2011), metazooplankton abundance and diversity (Nowaczyk et al., 2011), copepod parasites (Alves-de-Souza et al., 2011).

The P depletion of the MS was confirmed particularly in the ultraoligotrophic eastern basin (Pujo-Pay et al., 2011) which definitively establishes the MS as one of the Low P Low Chlorophyll (LPLC) areas of the world ocean (Moutin et al., 2008). Following the nutriclines, parallel deep maxima of biogenic silica, of fucoxanthin, and of tchl-*a* (Crombet at al., 2011) were evidenced towards the East together with decreases in biomasses and production (Christaki et al., 2011; Crombet et al., 2011; Lamy et al., 2011; Nowaczyk et al., 2011; Van Wambeke et al., 2011). Contrary to the Deep Chlorophyll Maximum which was a persistent feature of the MS, the Deep Silica Maximum correlated with the Deep Fucoxanthin Maximum as was observed in discrete areas of each basin (Crombet et al., 2011). Interestingly, there was an eastward decreasing trend of N_2 fixation, the results of which disagree with indirect estimates based on geochemical tracers and nitrogen budget (Bonnet et al., 2011). The majority of identified diazotrophs were isolated unicellular diazotrophic cyanobacteria of the picoplanktonic size fraction (Le Moal et al., 2011). Nevertheless, those living in association with diatoms were observed at nearly all sites (Crombet et al., 2011) giving an unexpected yet interesting coupling between the nitrogen and silicon cycles in the MS. Dissolved carbon production increases under strong nutrient limitation (Lopez-Sandoval et al., 2011), which may also explain the stronger DOC accumulation in the east and inside the eddies (Pujo-Pay et al., 2011, see Sect. 5.4). Phospholipid concentration was found to correlate with phosphate concentration across the MS, and a rapid response of membrane lipid composition to changes in nutrients was demonstrated for the first time (Popendorf et al., 2011). The on board measurements

BGD
8, 8091–8160, 2011

of cell-specific radiolabeled leucine using flow cytometry coupled with cell sorting allowed to reinforce the prevalent role of mixotrophs within the microbial communities of the MS (Talarmin et al., 2011). It was shown that dinospores were able to thrive and infect dinoflagellates, both in coastal and ultraoligotrophic waters, emphasizing the overlooked role of parasitism in food web and biogeochemical cycles (Siano et al., 2011). No large differences in the genetic diversity of the cyanobacterial populations observed during the BOUM cruise (2008) and the previous PROSOPE cruise (1999) were observed, suggesting that local populations have not yet been displaced by their (sub)tropical counterparts (Mella-Flores et al., 2011). The three geographically distant eddies showed very different biogeochemical conditions from the typical East-West trends in the MS (Pujo-Pay et al., 2011) and different ecosystems from surrounding waters (Christaki et al., 2011) probably principally because of the "closed" system conditions they experienced from the previous winter (see Sect. 5.4). They were chosen for process studies.

2. Process studies at the centre of the three anticyclonic eddies studied.

   Process studies concern both in situ measurements and microcosm experiments. The first estimations of turbulent dissipation inside anticyclonic eddies evidence a significant increase at the top and base of eddies which can be associated with strong near-inertial waves (Cuypers et al., 2011). Vertical turbulent diffusivity is increased both in these regions and in the weakly stratified eddy core (Cuypers et al., 2011). This allows the quantification of nitrate flux by upward diffusion, which was low and of the same order of magnitude as input by N_2 fixation (Bonnet et al., 2011). Contrary to the common view that siliceous phytoplankton are not key players in the MS, Crombet et al. (2011) suggest that they may contribute in a major way to marine production. Bio-optical anomaly and diurnal variability of the particulate matter were studied. For the first time, the diel cycle of the particulate backscattering coefficient was observed from field measurements (Loisel et al., 2011). A new method for analysing diel cycles in particulate beam-attenuation coefficient measured at multiple wavelengths suggests that most of the observed

BGD
8, 8091–8160, 2011

variations can be ascribed to a synchronized population of cells with an equivalent spherical diameter of between 1–4 µM (Dall'Olmo et al., 2011). Nutrient limitation of the pelagic microbial food web was investigated using amended microcosm experiments. A gap between biogeochemical features (an apparent P-starved status) and biological responses (no apparent P-limitation) was demonstrated (Tanaka et al., 2011) as well as an uncoupling of phytoplankton production and consumption by heterotrophic prokaryotes (Lagaria et al., 2011). Primary production significantly increased after addition of aerosols, indicating the relieving of on-going (co)-limitation (Ternon et al., 2011) and the strong stimulation of N_2 fixation (Ridame et al., 2011).

3. Representation of the main biogeochemical fluxes and the dynamics of the planktonic trophic network.

   An interesting schematic box-plot representation of the biogeochemical functioning of the two Mediterranean basins was proposed by Pujo-Pay et al., (2011). Surprisingly, the nitrate vs. phosphate ratio in the intermediate and deep layer tended towards the canonical Redfield values in both basins and their biogeochemical functioning showed a similar pattern. A multi-element model using Eco3M (Ecological Mechanistic Modular tool) was implemented to understand how primary producers and remineralisers interact and control the overall DOC and nutrients dynamics. It was suggested that the unusually high N:P ratio of the MS may favour the uncoupling between growth and carbon production, leading to higher DOC accumulation when compared to systems with lower N:P ratio (Mauriac et al., 2011a). The next step will be to use the numerous data collected during the BOUM cruise (http://www.obs-vlfr.fr/proof/php/x_datalist.php?xxop=boum\&xxcamp=boum) to implement physical models on the spatial scales of the eddy and of the whole MS, in order to study the influence exerted by the numerous anticyclonic eddies on anthropic carbon sequestration in the MS and on the decadal time scale.

BGD
8, 8091–8160, 2011

Supplementary material related to this article is available online at: http://www.biogeosciences-discuss.net/8/8091/2011/bgd-8-8091-2011-supplement.pdf.

Acknowledgements. This is a contribution of the BOUM (Biogeochemistry from the Oligotrophic to the Ultraoligotrophic Mediterranean) experiment (http://www.com.univ-mrs.fr/BOUM) of the French national LEFE-CYBER program, the European IP SESAME and the international IMBER project. The BOUM experiment was coordinated by the Institut des Sciences de l'Univers (INSU) and managed by the Centre National de la Recherche Scientifique (CNRS). The authors thank the crew of the R/V L'Atalante for their outstanding shipboard operations. Claudie Marec is warmly thanked for their efficient help in CTD rosette management and data processing as is Marie Paule Torre for the LEFE CYBER database management. Nathalie Leblond is acknowledged for her work on sediment trap. Martine Aperio and Catherine Perrot are acknowledged for the administrative work.

The publication of this article is financed by CNRS-INSU.

References

Alves-de-Souza, C., Cornet, C., Nowaczyk, A., Gasparini, S., Skovgaard, A., and Guillou, L.: Blastodinium spp. infect copepods in the ultra-oligotrophic marine waters of the Mediterranean Sea, Biogeosciences Discuss., 8, 2563–2592, doi:10.5194/bgd-8-2563-2011, 2011.

Ammerman, J. W., Hood, R. R., Case, D. A., and Cotner, J. B.: Phosphorus deficiency in the Atlantic: an emerging paradigm in oceanography, Eos Transactions, American Geophysical Union 84, 165–170, doi:10.1029/2003EO180001, 2003.

Antoine, D., André, J. m., and Morel, A.: Oceanic primary production : II. Estimation at global scale from satellite (Coastal Zone Color Scanner) chlorophyll, Global Biogeochem. Cy., 10, 57–69, 1996.
Avril, G.: DOC Dynamics in the northwestern Mediterranean Sea (DYFAMED site), Deep-Sea Res. Pt. II, 49, 2163–2182, 2002.
Benitez-Nelson, C. R.: The Biogeochemical Cycling of Phosphorus in Marine Systems, Earth Sci. Rev., 51, 109–135, 2000.
Benitez-Nelson, C. R. and McGillicuddy D. J.: Mesoscale Physical-Biological-Biogeochemical Linkages in the Open Ocean: An Introduction to the results of the E-Flux and EDDIES Programs (Preface), Deep-Sea Res. Pt. II, 55, 1133–1138, 2008.
Benson, B. B. and Krause, D.: The concentration and isotopic fractionation of oxygen dissolved in freshwater and seawater in equilibrium with the atmosphere, Limnol. Oceanogr., 29(3), 620–632, 1984.
Berland, B. R., Bonin, D. J., and Maestrini, S. Y.: Azote ou phosphore? Considérations sur le "paradoxe nutritionnel" de la mer méditerranée, Oceanol. Acta, 3, 135–141, 1980.
Bethoux, J. P., Morin, P., Madec, C., and Gentili, B.: Phosphorus and nitrogen behaviour in the Mediterranean Sea, Deep-Sea Res., 39, 1641–1654, 1988.
Bonin, D. J., Bonin, M. C., and Berman, T.: Mise en évidence expérimentale des facteurs nutritifs limitants de la production du micro-nanoplancton et de l'ultraplancton dans une eau côtière de la Méditerranée orientale (Haïfa, Israël), Aquatic Sci., 51, 132–148, 1989.
Bonnet, S., Grosso, O., and Moutin, T.: Planktonic dinitrogen fixation in the Mediterranean Sea: a major biogeochemical process during the stratified period?, Biogeosciences Discuss., 8, 1197–1225, doi:10.5194/bgd-8-1197-2011, 2011.
Boyd, P. W. and Doney, S. C.: The impact of climate change and feedback processes on the Ocean Carbon Cycle, in: Ocean Biogeochemistry – the role of the ocean carbon cycle in global change, edited by: M. J. R. Fasham, Springer-Verlag, Berlin, Germany, 157–187, 2003.
Brenner, S.: Long-term evolution and dynamics of a persistent warm core eddy in the eastern Mediterranean Sea, Deep-Sea Res. Pt. II, 40, 1193–1206, 1993.
Broecker, W. S.: Keeping global change honest, Global Biogeochem. Cy., 1, 15–29, 1991.
Chapman, R. and Nof, D.: The sinking of Warm-Core rings, J. Phys. Oceanog., 18, 4, 565–583, 1988.
Christaki, U., Van Wambeke, F., and Dolan, J. R.: Nanoflagellates (mixotrophs, heterotrophs

BGD
8, 8091–8160, 2011

and autotrophs) in the oligotrophic eastern Mediterranean: standing stocks, bacterivory and relationships with bacterial production, Mar. Ecol.-Prog. Ser., 181, 297–307, doi:10.3354/meps181297, 1999.
Christaki, U., Van Wambeke, F., Lefevre, D., Lagaria, A., Prieur, L., Pujo-Pay, M., Grattepanche, J.-D., Colombet, J., Psarra, S., Dolan, J. R., Sime-Ngando, T., Conan, P., Weinbauer, M. G., and Moutin, T.: Microbial food webs and metabolic state across oligotrophic waters of the Mediterranean Sea during summer, Biogeosciences, 8, 1839–1852, doi:10.5194/bg-8-1839-2011, 2011.
Claustre, H. and Maritorena, S.: The Many Shades of Ocean Blue, Science, 302, 1514–1515, 2003.
Copin-Montégut, G. and Avril, B.: Vertical distribution and temporal variation of dissolved organic carbon in the North-Western Mediterranean Sea, Deep-Sea Res., 40, 1963–1972, 1993.
Coste, B., Le Corre, P., and Minas, H. J.: Re-evaluation of the nutrient exchanges in the strait of Gibraltar, Deep-Sea Res., 35, 767–775, 1992.
Coste, B., Minas, H. J., and Bonin, M. C. : Proprités hydrologiques et chimiques des eaux du bassin Occidental de la Mediterranee, Campagne MEDIPROD 4. Publ., CNEXO, Ser. Result. Campagnes Mer., 26, 106 pp., 1984.
Crombet, Y., Leblanc, K., Quéguiner, B., Moutin, T., Rimmelin, P., Ras, J., Claustre, H., Leblond, N., Oriol, L., and Pujo-Pay, M.: Deep silicon maxima in the stratified oligotrophic Mediterranean Sea, Biogeosciences, 8, 459–475, doi:10.5194/bg-8-459-2011, 2011.
Cuypers, Y., Bouruet-Aubertot, P., Marec, C., and Fuda, J. L.: Characterization of turbulence and validation of fine-scale parametrization in the Mediterranean Sea during BOUM experiment, Biogeosciences Discuss., in preparation, 2011.
Dall'Olmo, G., Westberry, T. K., Behrenfeld, M. J., Boss, E., Courties, C., Prieur, L., Hardman-Mountford, N., and Moutin, T.: Inferring phytoplankton carbon and eco-physiological rates from diel cycles of spectral particulate beam-attenuation coefficient, Biogeosciences Discuss., 8, 3009–3050, doi:10.5194/bgd-8-3009-2011, 2011.
Defant, A.: Physical Oceanography, Pergamon, New York, USA, 1, 729 pp., 1961.
Deutsch, C., Sarmiento, J. L., Sigman, D. M., Gruber, N., and Dunne, J. P.: Spatial coupling of nitrogen inputs and losses in the ocean, Nature, 445, 163–167, 2007.
Diaz, F., Raimbault, P., Boudjellal, B., Garcia, N., and Moutin, T.: Early spring phosphorus limitation of primary productivity in a NW Mediterranean coastal zone (Gulf of Lions), Mar.

BGD
8, 8091–8160, 2011

Ecol. Progr. Ser., 211, 51–62, 2001.
Dolan, J. R., Claustre H., Carlotti F., Plounevez S., and Moutin, T.: Microzooplankton diversity: relationships of tintinnid ciliates with resources, competitors & predators from the Atlantic Coast of Morocco to the Eastern Mediterranean, Deep-Sea Res. I, 47, 1217–1234, 2002.
D'Ortenzio F. and Ribera d'Alcala, M.: On the trophic regimes of the Mediterranean Sea: a satellite analysis, Biogeosciences, 6(2), 139–148, 2009.
D'Ovidio, F., De Monte, S., Alvain, S., Dandonneau, Y., and Lévy, M.: Fluid dynamical niches of phytoplankton types, Proc. Natl. Acad. Sci. U.S. A., 107(43), 18366–18370, doi:10.1073/pnas.1004620107, 2010.
Dugdale, R. C. and Goering, J. J.: Uptake of new and regenerated forms of nitrogen in primary productivity, Limnol. Oceanogr., 12, 196–206, 1967.
Eppley, R. W. and Peterson, B. J.: Particulate organic matter flux and planktonic new production in the deep ocean, Nature, 282, 677–680, 1979.
Falkowski, P. G.: Evolution of the nitrogen cycle and its influence on the biological sequestration of CO_2 in the ocean, Nature, 327, 242–244, 1997.
Fusco, G., Manzella, G. M. R., Cruzado, A., Gacic, M., Gasparini, G. P., Kovacevic, V., Millot, C., Tziavos, C., Velasquez, Z. R., Walne, A., Zervakis, V., and Zodiatis, G.: Variability of mesoscale features in the Mediterranean Sea from XBT data analysis, Ann. Geophys., 21, 21–32, doi:10.5194/angeo-21-21-2003, 2003.
Garcia N., Raimbault, P., Gouze, E., and Sandroni, V.: Fixation de diazote et production primaire en méditerranée occidentale, C. R. Biol., 309, 742–750, 2006.
Gill, A. E.: Atmosphere-Ocean Dynamics, Academic Press, 662 pp., 1982.
Gregg, M. C.: Scaling turbulent dissipation in the thermocline, J. Geophys. Res., 94, 9686–9698, 1989.
Guerzoni, S., Chester, R., Dulac, F., Herut, B., Loÿe-Pilot, M. D., Measures, C., Migon, C., Molinaroli, E., Moulin, C., Rossini, P., Saydam, C., Soudine, A., and Ziveri, P.: The role of atmospheric deposition in the biogeochemistry of the Mediterranean Sea, Prog. Oceanogr., 44(1–3), 147–190, 1999.
Herbland, A. and Voituriez, B.: Production primaire, nitrate et nitrite dans l'Atlantique tropical. 1. Distribution du nitrate et production primaire, Cah. ORSTOM, Sér. Océanogr., 15, 47–56, 1977.
Herut, B., Zohary, T., Robarts, R. D., and Kress, N.: Adsorption of dissolved phosphate onto loess particles in surface and deep eastern Mediterranean water, Mar. Chem., 64(4), 253–

BGD
8, 8091–8160, 2011

265, 1999.
Jeanthon, C., Boeuf, D., Dahan, O., Le Gall, F., Garczarek, L., Bendif, E. M., and Lehours, A.-C.: Diversity of cultivated and metabolically active aerobic anoxygenic phototrophic bacteria along an oligotrophic gradient in the Mediterranean Sea, Biogeosciences, 8, 1955–1970, doi:10.5194/bg-8-1955-2011, 2011.
Kähler, P., Oschlies, A., Dietze, H., and Koeve, W.: Oxygen, carbon, and nutrients in the oligotrophic eastern subtropical North Atlantic, Biogeosciences, 7, 1143–1156, doi:10.5194/bg-7-1143-2010, 2010.
Karl, D. M. and Letelier, R. M.: Seascape microbial ecology: Habitat structure, biodiversity and ecosystem function, in: The Princeton Guide to Ecology, edited by: Levin, S. A., Princeton University Press, Princeton, New Jersey, USA, 488–500, 2009.
Karl, D.M., Michaels, A., Bergman, B., Capone, D. G., Carpenter, R. C., Letelier, R., Lipschultz, F., Paerl, H. W., Sigman, D. M., and Stal, L.: Dinitrogen fixation in the world's oceans, Biochemistry, 57–58, 47–98, 2002.
Karl, D. M., Laws, E. A., Morris, P., Williams, P. J. leB, and Emerson, S.: Metabolic balance of the open sea, Nature, 426, p. 32, 2003.
Kerhervé, P., Minagawa, M., Heussner, S., and Monaco, A.: Stable isotopes (13C/12C and 15N/14N) in settling organic matter of the northwestern Mediterranean Sea: biogeochemical implications, Oceanol. Acta, 24, supplement:S77–S85, 2001.
Kleypas J. A. and Langdon, C.: Coral reefs and changing seawater chemistry, Chapter 5 in: Coral Reefs and Climate Change: Science and Management, edited by: Phinney, J. T., Hoegh-Guldberg, O., Kleypas, J. A., Skirving, W., and Strong, A., AGU Monograph Series, Coastal and Estuarine Studies, Am. Geophys. Union, Washington DC, USA, 61, 73–110, 2006.
Krom, M. D., Kress, N., and Brenner, S.: Phosphorus limitation of primary productivity in the eastern Mediterranean Sea, Limnol. Oceanogr., 36, 424–432, 1991.
Krom, M. D., Brenner, S., Kress, N., Neori, A., and Gordon, L. I.: Nutrient dynamics and new production in a warm-core eddy from the E. Mediterranean, Deep-Sea Res., 39, 467–480, 1992.
Krom, M. D., Thingstad, T. F., Carbo, P., Herut, B., Kress, N., Flaten, G. A. F., Skjoldal, E. F., Tanaka, T., Mantoura, R. F. C., Tselipides, T., Pitta, P., Psarra, S., Polychronaki, T., Rassoulzadegan, F., Law, C. S., Groom, S., Woodward, E. M. S., Liddicoat, M. I., Fileman, T. W., Zohary, T., Spyres, G., Wassmann, P., Wexels-Riser, C., Zodiatis, G., Drakopoulos, P.:

BGD
8, 8091–8160, 2011

Summary and overview of the CYCLOPS P addition Lagrangian experiment in the eastern Mediterranean, Deep-Sea Res. II, 52, 3090–3108, doi:10.1016/j.dsr22005.08.018, 2005a.
Krom, M. D., Woodward, E. M. S., Herut, B., Kress, N., Carbo, P., Mantoura, R. F. C., Spyres, G., Thingstad, T. F., Wassmann, P., Wexels-Riser, C., Kitidis, V., Law, C., and Zodiatis, G.: Nutrient cycling in the south east Levantine basin of the eastern Mediterranean: results from a phosphorus starved system, Deep-Sea Res. I, 52, 2879–2896, 2005b.
Krom, M.D., Emeis, K. C., Van Cappellen, P.: Why is the Western Meditteranean phosphorus limited?, Prog. Oceanogr., 85, 236–244, 2010.
Lacombe, H. and Tchernia, P. : Caractères hydrologiques et circulation des eaux en méditerranée, in: The Mediterranean sea, edited by: Stanley, D. J., Dowden Hutchinson RossInc., Stroudsburg, 26–36, 1972.
Lacombe H., Tchernia, P., and Gamberoni, L.: Variable nottom water in the Western Mediterranean Basin, Prog. Oceanog. 14, 319–338, 1985.
Lagaria, A., Psarra, S., Lefèvre, D., Van Wambeke, F., Courties, C., Pujo-Pay, M., Oriol, L., Tanaka, T., and Christaki, U.: The effects of nutrient additions on particulate and dissolved primary production in surface waters of three Mediterranean eddies, Biogeosciences Discuss., 7, 8919–8952, doi:10.5194/bgd-7-8919-2010, 2010.
Lamy, D., Jeanthon, C., Cottrell, M. T., Kirchman, D. L., Van Wambeke, F., Ras, J., Dahan, O., Pujo-Pay, M., Oriol, L., Bariat, L., Catala, P., Cornet-Barthaux, V., and Lebaron, P.: Ecology of aerobic anoxygenic phototrophic bacteria along an oligotrophic gradient in the Mediterranean Sea, Biogeosciences, 8, 973–985, doi:10.5194/bg-8-973-2011, 2011.
Lascaratos A., Willimams, R. G., and Tragou E.: A mixed-Layer study of the formation of Levantine Intermediate Water, J. Geophys. Res., 98, C8, 14739–14749, 1993.
Le Quéré, C., Raupach, M. R., Canadell, J. G., Marland, G., Bopp, L., Ciais, P., Conway, T. J., Doney, S. C., Feely, R., Foster, P., Friedlingstein, P., Gurney, K., Houghton, R. A., House, J. I., Huntingford, C., Levy, P. E., Lomas, M. R., Majkut, J., Metzl, N., Ometto, J. P., Peters, G. P., Prentice, I. C., Randerson, J. T., Running, S. W., Sarmiento, J. L., Schuster, U., Sitch, S., Takahashi, T., Viovy, N., van der Werf, G. R., and Woodward, F. I.: Trends in the sources and sinks of carbon dioxide, Nat. Geosci., 2, 831–836, doi:10.1038/ngeo689, 2009.
Le Moal, M., Collin, H., and Biegala, I. C.: Intriguing diversity among diazotrophic picoplankton along a Mediterranean transect: a dominance of rhizobia, Biogeosciences, 8, 827–840, doi:10.5194/bg-8-827-2011, 2011.
Leblanc, K., Queguiner, B., Garcia, N., Rimmelin, P., and Raimbault, P.: Silicon cycle in the

BGD
8, 8091–8160, 2011

Northwestern Mediterranean sea: seasonnal study of a coastal oligotrophic site, Oceanol. Acta, 26, 339–356, 2003.
Lévy, M.: The modulation of biological production by oceanic mesoscal turbulence, Lect. Notes Phys., Transport in Geophysical flow: Ten years after, edited by: Weiss, J. B. and Provenzale, A., Springer, 744, 219–261, doi:10.1007/978-3-540-75215-8_9, 2008.
Loisel, H. and Morel, A.: Light scattering and chlorophyll concentration in case 1 waters: a re-examination, Limnol. Oceanogr., 43, 847–857, 847–858, 1998.
Loisel, H., Vantrepotte, V., Norkvist, K., Mériaux, X., Kheireddine, M., Ras, J., Pujo-Pay, M., Combet, Y., Leblanc, K., Mauriac, R., D. Dessailly, D., and Moutin, T.: Characterization of the bio-optical anomaly and diurnal variability of the particulate matter in ultraoligotrophic eddies of the Mediterranean Sea, Biogeosciences Discuss., in preparation, 2011.
Lomas, M. W., Burke, A. L., Lomas, D. A., Bell, D. W., Shen, C., Dyhrman, S. T., and Ammerman, J. W.: Sargasso Sea phosphorus biogeochemistry: an important role for dissolved organic phosphorus (DOP), Biogeosciences, 7, 695–710, doi:10.5194/bg-7-695-2010, 2010.
López-Sandoval, D. C., Fernández, A., and Marañón, E.: Dissolved and particulate primary production along a longitudinal gradient in the Mediterranean Sea, Biogeosciences, 8, 815–825, doi:10.5194/bg-8-815-2011, 2011.
Ludwig, W., Dumont, E., Meybeck, M., and Heussner, S.: River discharges of water and nutrients to the Mediterranean and Black Sea: Major drivers for ecosystem changes during past and future decades?, Prog. Oceanogr., 80, 199–207, doi:10.1016/j.pocean.2009.02.001, 2009.
Marañón, E., Cermeño, P., and Pérez, V.: Continuity in the photosynthetic production of dissolved organic carbon from eutrophic to oligotrophic waters, Mar. Ecol.-Prog. Ser., 299, 7–17, 2005.
Markaki, Z., Loye-Pilot, M. D., Violaki, K., and Mihalopoulos, N.: Variability of atmospheric deposition of dissolved nitrogen and phosphorus in the Mediterranean and possible link to the anomalous seawater N/P ratio, Mar. Chem., 120, 187–194, 2010.
Mauriac, R., Moutin, T., and Baklouti, M.: Accumulation of DOC in Low Phosphate Low Chlorophyll (LPLC) area: is it related to higher production under high N:P ratio?, Biogeosciences, 8, 933–950, doi:10.5194/bg-8-933-2011, 2011.
Mauriac, R., Moutin, T., Talarmin, A., Marie, D., Cornet-Barthaux, V., Pujo-Pay, M., Oriol, L., and Gargzarek, L.: Short-term temporal trends and coupling between picoplankton C-P biomass and prodution in the Mediterranean Sea, Biogeosciences Discuss., accepted, 2011b.

BGD
8, 8091–8160, 2011

Mc Gill, D. A.: A preliminary study of the oxygen and phosphate distribution in the Mediterranean Sea. Deep Sea res., 8, 259–269, 1961.
Mc Gill, D. A.: The relative supplies of phosphate, nitrate and silicate in the Mediterranean Sea, Comm. Int. Mer Medit., 18, 737–744, 1965.
McGillicuddy Jr., D. J., Johnson R., Siegel D. A., Michaels A . F., Bates N. R., and Knap A. H.: Mesoscale variations of biogeochemical properties in the Sargasso Sea, J. Geophys. Res., 104(C6), 13,381–13,394, 1999.
Mella-Flores, D., Mazard, S., Humily, F., Partensky, F., Mahé, F., Bariat, L., Courties, C., Marie, D., Ras, J., Mauriac, R., Jeanthon, C., Bendif, E. M., Ostrowski, M., Scanlan, D. J., and Garczarek, L.: Is the distribution of Prochlorococcus and Synechococcus ecotypes in the Mediterranean Sea affected by global warming?, Biogeosciences Discuss., 8, 4281–4330, doi:10.5194/bgd-8-4281-2011, 2011.
Minas, H. J., Minas, M., Coste, B., Gostan, J., Nival, P., and Bonin, M. C.: Production de base et de recyclage; une revue de la problématique en Méditerranée nord-occidentale, no spécial: Océanographie pélagique méditerranéenne, Minas et Nival (eds), Oceanol. Acta, 155–162, 1988.
Montoya, J. P., Holl, C. M., Zehr, J. P., Hansen, A., Villareal, T. A., and Capone, D. G.: High rates of N_2 fixation by unicellular diazotrophs in the oligotrophic Pacific Ocean, Nature, 430, 1027–1032, 2004.
Morel, A. and Maritorena, S.: Bio-optical properties of oceanic waters: A reappraisal, J. Geophys. Res., 106, 7763–7780, 2001.
Moutin, T. : Cycle biogéochimique du phosphate: rôle dans le contrôle de la production planctonique et conséquences sur l'exportation de carbone de la couche éclairée vers l'océan profond, Océanis, 36–4, 2000.
Moutin, T. and Raimbault, P.: Primary production, carbon export and nutrients availability in western and eastern Mediterranean Sea in early summer 1996 (MINOS cruise), J. Marine Syst., 33/34, 273–288, 2002.
Moutin, T., Raimbault, P., and Poggiale, J. C. : Production primaire dans les eaux de surface de la méditerranée occidentale: Calcul de la production journalière, C. R. Acad. Sci. Paris, Sciences de la vie, 322, 651–659, 1999.
Moutin, T., Thingstad, T. F., Van Wambeke, F., Marie, D., Slawyk, G., Raimbault, P., and Claustre, H.: Does competition for nano-molar phosphate supply explain the predominance of the cyanobacterium Synechococcus?, Limnol. Oceanogr., 47, 1562–1567, 2002.

BGD
8, 8091–8160, 2011

Moutin, T., Van Den Broeck, N., Beker, B., Dupouy, C., Rimmelin, P., and Le Bouteiller, A.: Phosphate availability controls Trichodesmium spp. biomass in the SW Pacific ocean, Mar. Ecol. Progr. Ser., 297, 15–21, 2005.

Moutin, T., Karl, D. M., Duhamel, S., Rimmelin, P., Raimbault, P., Van Mooy, B. A. S., and Claustre, H.: Phosphate availability and the ultimate control of new nitrogen input by nitrogen fixation in the tropical Pacific Ocean, Biogeosciences, 5, 95–109, 2008, http://www.biogeosciences.net/5/95/2008/.

Murnane, R., Sarmiento, J. L., and Le Quéré, C. L.: Spatial distribution of air-sea CO_2 fluxes and the interhemispheric transport of carbon by the oceans, Glob. Biogeochem. Cy., 13, 287–305, 1999.

Nowaczyk, A., Carlotti, F., Thibault-Botha, D., and Pagano, M.: Metazooplankton diversity, community structure and spatial distribution across the Mediterranean Sea in summer: evidence of ecoregions, Biogeosciences Discuss., 8, 3081–3119, doi:10.5194/bgd-8-3081-2011, 2011.

Osborn, T. R.: Estimates of the local rate of vertical diffusion from dissipation measurements, J. Phys. Oceanogr., 10, 83–89, 1980.

Pantoja, S., Repeta, D. J., Sachs, J. P., and Sigman, D. M.: Stable isotope constraints on the nitrogen cycle of the Mediterranean Sea water column, Deep Sea Res. Part I, 49(9), 1609–1621, 2002.

Pingree R. D. and Le Cann, B.: Anticyclonic Eddy X91 in the Southern Bay of Biscay, May 1991 to February 1992, J. Geophys. Res., 97, C11, 14353–14367, 1992.

Pingree R. D. and Le Cann, B.: A Shallow Meddy (A Smeddy) From the Secondary Mediterranean Salinity Maximum, J. Geophys. Res., 98, C11, 20169–20185, 1993.

Popendorf, K. J., Tanaka, T., Conan, P., Courties, C., Lagaria, A., Moutin, T., Oriol, L., Pujo-Pay, M., Sofen, L., Van Mooy, B. A. S.: Intact polar diacylglycerolipid changes in response to nutrient limitation in the Mediterranean Sea, Biogeosciences Discuss., in preparation, 2011.

Puillat, I., Taupier-Letage, I., and Millot, C.: Algerian Eddies lifetime can near 3 years, J. Marine Syst., 31, 245–259, 2002.

Pujo-Pay, M., Conan, P., Oriol, L., Cornet-Barthaux, V., Falco, C., Ghiglione, J.-F., Goyet, C., Moutin, T., and Prieur, L.: Integrated survey of elemental stoichiometry (C, N, P) from the western to eastern Mediterranean Sea, Biogeosciences, 8, 883–899, doi:10.5194/bg-8-883-2011, 2011.

Raimbault, P. and Coste, B.: Very high values of nitrate:phosphate ratio (>30) in the subsurface

BGD
8, 8091–8160, 2011

layers of the western Mediterranean Sea, Rapp. Comm. Int. Mer. médit., 32, C-18, 1990.
Redfield, A. C., Ketchum, B. H., and Richards, F. A.: The influence of organisms on the composition of sea water, in: The Sea, ideas and observations on progress in the study of the sea, edited by: Hill, M.M., 2, J. Wiley and Sons, New York, USA, 26–77, 1963.
Ridame, C., Moutin, T., and Guieu, C.: Does phosphate adsorption onto Saharan dust explain the unusual N/P ratio in the Mediterranean Sea?, Oceanol. Acta, 26(5), 629–634, 2003.
Ridame, C., Le Moal, M., Guieu, C., Ternon, E., Biegala, I. C., L'Helguen, S., and Pujo-Pay, M.: Nutrient control of N_2 fixation in the oligotrophic Mediterranean Sea and the impact of Saharan dust events, Biogeosciences Discuss., 8, 2629–2657, doi:10.5194/bgd-8-2629-2011, 2011.
Robinson A. R., Golnaraghi M., Leslie W. G., Artegiani A., Hecht A., Lazzon E., Michelato A., Sansone E., Theocharls A., and Ünlüata, Ü.: The eastern Mediterranean general circulation: features, structure and variability, Dynam. Atmos. Oceans, 15, 215–240, 1991.
Roether, W., Manca, B. B., Klein, B., Bregant, D., Georgopoulos, D., Beitzel, V., Kovacevich, V., and Luchetta, A.: Recent changes in Eastern Mediterranean deep waters, Science, 271, 333–335, 1996.
Sabine, C. L., Feely, R. A., Gruber, N., Key, R. M., Lee, K., and Bullister, J. L.: The oceanic sink for anthropogenic CO_2, Science, 305, 367–371, 2004.
Sachs J. P. and Repeta, D. J.: Oligotrophy and nitrogen fixation during eastern Mediterranean sapropel events, Science, 286, 2485–2488, 1999.
Sala, M. M., Peters, F., Gasol, J. M., Pedros-Alio, C., Marrasse, C., and Vaque, D.: Seasonal and spatial variations in the nutrient limitation of bacterioplankton growth in the northwestern Mediterranean, AME, 27, 47–56, 2002.
Sarmiento, J. L. and Gruber, N.: Ocean Biogeochemical Dynamics, Princeton University Press, Princeton, 503 pp., 2006.
Serret, P., Fernandez, E., Robinson, C. E. Malcolm S. Woodward, M. S., and Perez, V.: Local production does not control the balance between plankton photosynthesis and respiration in the open Atlantic Ocean, Deep-Sea Res. II 53, 1611–1628, 2006.
Siano, R., Alves-de-Souza, C., Foulon, E., Bendif, El M., Simon, N., Guillou, L., and Not, F.: Distribution and host diversity of Amoebophryidae parasites across oligotrophic waters of the Mediterranean Sea, Biogeosciences, 8, 267–278, doi:10.5194/bg-8-267-2011, 2011.
Siokou-Frangou, I., Christaki, U., Mazzocchi, M. G., Montresor, M., Ribera d'Alcalá, M., Vaqué, D., and Zingone, A.: Plankton in the open Mediterranean Sea: a review, Biogeosciences, 7,

BGD
8, 8091–8160, 2011

1543–1586, doi:10.5194/bg-7-1543-2010, 2010.
Talarmin, A., Van Wambeke, F., Catala, P., Courties, C., and Lebaron, P.: Flow cytometric assessment of specific leucine incorporation in the open Mediterranean, Biogeosciences, 8, 253–265, doi:10.5194/bg-8-253-2011, 2011.
Tanaka, T., Thingstad, T. F., Christaki, U., Colombet, J., Cornet-Barthaux, V., Courties, C., Grattepanche, J.-D., Lagaria, A., Nedoma, J., Oriol, L., Psarra, S., Pujo-Pay, M., and Van Wambeke, F.: Lack of P-limitation of phytoplankton and heterotrophic prokaryotes in surface waters of three anticyclonic eddies in the stratified Mediterranean Sea, Biogeosciences, 8, 525–538, doi:10.5194/bg-8-525-2011, 2011.
Taupier-Letage, I.: On the use of thermal images for circulation studies: Application to the eastern Mediterranean basin, in: Remote Sensing of the European Sea, edited by: Barale, V. and Gade, M., Springer Verlag, Berlin, 153–164, 2008.
Ternon, E., Guieu, C., Ridame, C., L'Helguen, S., and Catala, P.: Longitudinal variability of the biogeochemical role of Mediterranean aerosols in the Mediterranean Sea, Biogeosciences, 8, 1067–1080, doi:10.5194/bg-8-1067-2011, 2011.
Thingstad, T. F.: A theoretical approach to structuring mechanisms in the pelagic food web, Hydrobiologia, 363, 59–72, 1998.
Thingstad, T. F., Skjoldal, E. F., and Bohne. R. A.: Phosphorus cycling and algal-bacterial competition in Sandsfjord, western Norway, Mar. Ecol.-Prog. Ser., 99, 239–259, 1993.
Thingstad, T. F., Hagström A. and Rassoulzadegan, F.: Accumulation of degradable DOC in surface waters: Is it caused by a malfunctioning microbial loop? Limnol. Oceanogr., 42, 398–404, 1997.
Thingstad, T. F., Krom, M. D., Mantoura, R. F. C., Flaten, G. A. F., Groom, S., Herut, B., Kress, N., Law, C., Pasternak, A., Pitta, P., Psarra, S., Rassoulzadegan, F., Tanaka, T., Tselipides, A., Wassmann, P., Woodward, E. M. S., Wexels Riser, C., Zodiatis, G., and Zohary, T.: Nature of P limitation in the ultraoligotrophic Eastern Mediterranean, Science, 309, 1068–1071, 2005.
Van Wambeke, F., Christaki, U., Giannakourou, A., Moutin, T., and Souvemerzoglou, K.: Longitudinal and vertical trends of bacterial limitation by phosphorus and carbon in the Mediterranean sea, Microb. Ecol., 43, 119–133, 2002.
Van Wambeke, F., Catala, P., Pujo-Pay, M., and Lebaron, P.: Vertical and longitudinal gradients in HNA-LNA cell abundances and cytometric characteristics in the Mediterranean Sea, Biogeosciences, 8, 1853–1863, doi:10.5194/bg-8-1853-2011, 2011.

BGD
8, 8091–8160, 2011

Vaulot, D., Lebot, N., Marie, D., and Fukai, E.: Effect on phosphorus on the Synechococcus cell cycle i,n Surface Mediterranean Waters during Summer, Appl. Environ. Microb., 62, 2527–2533, 1996.

Williams, P. J. leB., Morris P. J., and Karl, D. M.: Net community production and metabolic balance at the oligotrophic ocean site, station ALOHA, Deep-Sea Research I, 51, 1563–1578, 2004.

Zehr, J. P., Waterbury, J. B., Turner, P. J., Montoya, J. P., Omoregle, E., Steward, G. F., Hansen, A., and Karl, D. M.: Unicellular cyanobacteria fix N_2 in the subtropical North Pacific ocean, Nature, 412, 635–638, 2001.

Zohary, T. and Robarts, R. D.: Experimental study of microbial P limitation in the Eastern Mediterranean, Limnol. Oceanogr., 43, 387–395, 1998.

BGD

8, 8091–8160, 2011

Table 1a. Date, location and general biogeochemical characteristics of the stations investigated along the BOUM transect. Distance (km) : Distance from the Rhône river mouth (SD27); $MLD_{0.03}$: Mixed Layer $Depth_{0.03}$ (m) : depth where $\rho > \rho_{0m} + 0.03\,kg\,m^{-3}$; MLD_{2d}: Mixed Layer Depth 2 days lagged (dbar); W-MLD :Winter Maximum Mixed Layer Depth (dbar); EZD, Euphotic Zone Depth (dbar) estimated according to Morel and Maritorena (2001); EZD, Mean and SD of the Euphotic Zone Depth (dbar): depth where I = 0.01*SPAR.

Station		CTD cast	Date	Latitude			Longitude			Bottom Depth (m)	Distance (km)	MLD 0.03 (dbar)	MLD 2d (dbar)	MLD W (dbar)	EZD (dbar)	EZD (dbar)
27	SD	193	18 July	43	12.70	N	4	55.80	E	105	0	2.0	2.5	98.0	76	
26	SD	192	18 July	42	37.00	N	4	57.30	E	1721	67	6.7	16.5	1000.0	87	
25	SD	190	18 July	41	59.80	N	5	0.00	E	2258	136	28.3	29.5	178.5	53	
24	SD	188	17 July	41	5.30	N	5	3.40	E	2663	237	8.9	15.5	104.5	77	
23	SD	187	17 July	40	10.70	N	5	6.70	E	2786	338	20.6	22.5	66.5	85	
A	LD	186	11–17 July	39	5.96	N	5	21.00	E	2758	433	7.8	13.5	90.5	102	83 ± 2
22	SD	130	11 July	38	53.70	N	6	45.08	E	2864	575	2.5	14.5	57.5	83	
21	SD	128	11 July	38	37.85	N	7	54.58	E	2159	679	9.7	16.5	58.5	92	
20	SD	127	10 July	38	21.80	N	9	3.90	E	1758	784	8.3	12.5	70.5	81	
19	SD	125	10 July	38	5.90	N	10	13.40	E	519	889	5.4	12.5	58.5	79	
18	SD	124	9 July	37	49.90	N	11	23.00	E	771	995	2.8	15.5	68.5	77	
17	SD	122	9 July	37	10.00	N	12	0.08	E	117	1087	5.5	23.5	56.5	86	
16	SD	121	9 July	36	3.93	N	12	48.06	E	861	1229	7.7	9.5	81.5	95	
15	SD	119	8 July	35	40.45	N	14	6.00	E	588	1354	4.4	11.5	65.5	101	
14	SD	118	8 July	35	17.00	N	15	24.10	E	382	1480	4.3	11.5	67.5	109	
13	SD	116	7 July	34	53.50	N	16	42.00	E	2097	1606	4.4	7.5	85.5	107	
12	SD	115	7 July	34	30.13	N	18	0.02	E	3321	1732	3.9	7.5	82.5	114	
B	LD	114	3–7 July	34	8.20	N	18	26.70	E	3070	1810	7.2	8.5	109.5	117	104 ± 4
1	SD	2	21 June	34	19.66	N	19	49.20	E	3210	1939	12.2	14.5	89.5	87	
2	SD	4	21 June	34	15.57	N	20	59.12	E	2593	2046	10.7	13.5	97.5	107	
3	SD	5	21 June	34	10.90	N	22	9.50	E	2382	2155	16.4	18.5	81.5	99	
4	SD	7	22 June	34	7.00	N	23	19.67	E	2471	2262	16.4	17.5	80.5	107	
5	SD	8	22 June	34	2.70	N	24	29.80	E	2616	2370	9.7	17.5	84.5	106	
6	SD	10	23 June	33	58.49	N	25	40.06	E	2761	2478	9.7	13.5	221.5	115	
7	SD	11	23 June	33	54.20	N	26	50.20	E	2784	2586	10.9	24.5	94.5	101	
8	SD	13	23 June	33	49.90	N	28	0.30	E	2768	2694	10.2	23.5	75.5	109	
9	SD	14	24 June	33	45.70	N	29	10.50	E	3033	2803	11.1	17.5	90.5	120	
10	SD	16	24 June	33	41.90	N	30	9.60	E	2942	2894	4.0	14.5	88.5	119	
11	SD	17	25 June	33	34.82	N	31	56.04	E	2514	3058	9.3	12.5	153.5	113	
C	LD	71	25–30 June	33	37.50	N	32	39.20	E	923	3130	10.1	11.5	396.5	103	102 ± 3

BGD
8, 8091–8160, 2011

Table 1b. Other general biogeochemical characteristics of the stations investigated along the BOUM transect. DCMD, Deep Chlorophyll Maximum Depth: depth where in vivo fluorescence sensor CTD reaches a maximum value; DCMC, Deep Chlorophyll Maximum Concentration: chl-*a* concentration at the DCMD (mg m^{-3}). Fluorescence Units were converted to total chl-*a* (tchl-*a*) concentration using the best fitted linear relationship between Fluorescence Units and direct HPLC total chl-*a* measurements ($r^2 = 0.98$, N = 79); Ichlo-*a*, Integrated total chl-*a* concentration (mg m^{-2}) between 0–150 dbar (for bottom depth < 150 dbar, the integration was performed from 0 to bottom depth minus 6 dbar); INO_3 and IPO_4: Integrated (0–150 dbar) nitrate and phosphate concentrations (mmol m^{-2}); D_x, S_x, N_x and r_x^2: characteristics of nutriclines (slopes in nM m^{-1} and depth in m where NO_3 or PO_4 reaches zero, N: number of samples for the linear relationship, r^2: correlation coefficient). All 0–500 m CTD casts were considered for the calculations at the LD stations; $DTPO_4$: depths before (°) and after (+) a large (> 100 h) increase of phosphate turnover time.

Station		DCMD (m)	DCMC (mg m^{-3})	Ichlo-*a* (mg m^{-2})	INO_3 (mmol m^{-2})	IPO_4 (mmol m^{-2})	D_{NO_3} (m)	S_{NO_3} (µmol m^{-4})	N_{NO_3}	$r_{NO_3}{}^2$	D_{PO_4}	S_{PO_4} (µmol m^{-4})	N_{PO_4}	$r_{PO4}{}^2$	$D_{TPO_4}{}^\circ$ (m)	$D_{TPO_4}{}^+$ (m)
27	SD			27.1	153.6	4.1	25	49.4	5	0.96	17	1.0	9	0.68	31	40
26	SD	40	1.7	34.2	846.4	29.9	19	144.1	3	0.89	23	5.0	3	1.00	25	51
25	SD	50	1.7	36.2	662.3	24.3	45	149.9	3	0.93	41	4.7	3	0.99	nm	nm
24	SD	70	0.75	38.8	327.3	8.5	58	79.8	3	0.85	68	2.6	3	0.91	76	101
23	SD	75	0.72	27.6	313.3	6.1	50	66.0	3	1.00	80	2.3	5	0.98	74	101
A	LD	85	0.7	22.7	49.0	2.2	72	11.8	98	0.76	nc	nc	nc	nc	76	91
22	SD	70	0.75	24.4	376.0	15.4	58	93.0	3	0.89	56	3.4	3	0.83	50	75
21	SD	80	0.45	23.0	312.7	14.5	67	92.3	3	0.84	60	3.0	3	0.83	nm	nm
20	SD	70	1.17	37.9	347.9	16.1	67	111.0	3	0.92	61	3.6	3	1.00	75	100
19	SD	65	1.05	32.9	432.7	15.5	50	105.6	3	1.00	47	2.8	3	0.80	nm	nm
18	SD	80	2	52.6	86.1	2.5	104	17.5	6	0.96	99	1.6	5	0.89	nm	nm
17	SD	80	0.77	25.7	57.0	2.1	73	123.9	5	0.85	71	3.4	5	0.84	nm	nm
16	SD	75	0.63	30.6	117.7	3.9	70	34.0	6	0.99	67	1.0	6	0.98	76	100
15	SD	100	0.43	25.0	58.1	2.7	97	41.1	6	0.99	84	1.1	6	0.97	75	101
14	SD	120	0.25	18.2	42.5	3.4	103	55.6	7	0.98	79	1.0	7	0.93	75	100
13	SD	90/140	0.62/0.70	33.3	79.0	3.3	80	35.7	6	0.94	84	1.3	5	0.91	73	123
12	SD	70/125	0.18–0.25	20.8	16.7	0.6	104	17.5	5	0.98	nc	nc	nc	nc	101	125
B	LD	75/140	0.15/0.26	19.7	7.4	0.0	114	15.5	96	0.92	nc	nc	nc	nc	121	141
1	SD	75/85	0.68	32.6	22.6	0.0	104	17.5	4	0.99	nc	nc	nc	nc	101	126
2	SD	110	0.32	20.0	57.9	0.5	98	36.8	5	0.99	109	0.8	5	0.93	100	125
3	SD	110	1.55	31.8	141.8	2.3	88	48.1	4	0.91	102	1.3	4	0.83	100	125
4	SD	105	0.4	21.8	161.5	3.1	91	49.4	4	0.95	106	1.4	4	0.93	101	126
5	SD	115	0.62	26.0	100.7	1.2	92	56.8	3	0.99	103	1.2	3	0.96	100	126
6	SD	110	0.42	22.6	23.9	0.5	96	15.9	3	1.00	nc	nc	nc	nc	125	251
7	SD	100	0.4	21.8	84.7	1.6	94	51.7	3	0.98	nc	nc	nc	nc	100	125
8	SD	90/100	0.50/0.35	20.6	128.5	2.5	77	51.6	3	0.99	nc	nc	nc	nc	100	125
9	SD	125	0.35	18.2	10.9	0.0	95	6.9	5	0.96	nc	nc	nc	nc	nm	nm
10	SD	110	0.32	15.5	28.3	0.5	78	12.6	3	0.98	nc	nc	nc	nc	100	126
11	SD	110	0.35	20.1	27.6	0.6	88	12.1	3	0.87	nc	nc	nc	nc	100	125
C	LD	110	0.62	25.1	32.4	8.3	93	24.9	71	0.64	nc	nc	nc	nc	101	120

nc: not calculated (linear relationship not established), nm: not measured

BGD
8, 8091–8160, 2011

Table 2. ARGO floats deployed along the BOUM transect at the three pre-defined LD stations (A, B, C).

			Deployment location	
Station	Float number	Date of deployment	Latitude	Longitude
A	WMO 6900664	17 July	39° 20.48° N	5 11.41 E
B	(Pro Bio A) WMO 6900674	4 July	34° 7.97° N	18° 26.70 E
B	WMO 6900663	7 July	33° 56.87° N	18° 27.29° E
C	(Pro Bio B) WMO 6900679	26 June	33° 37.53° N	32° 39.70 E
C	WMO 6900665	30 June	33° 42.54° N	32° 41.90 E

BGD
8, 8091–8160, 2011

Table 3. Specific depth characteristics of the three studied eddies at the three LD stations A(130; 186), B(2,71) and C(17,71). Numbers in brackets correspond to CTD casts "in" (i.e. near eddy axis) and "out", respectively. As eddy B shows, two halostads/pycnostads and an S anomaly (S Ano) sign change, two parts, surface and deep, were distinguished. General characteristics: D_{bottom} (bottom depth "in", see Table 1a), D_{range} (Range of depth where eddy influence is marked on any or some properties; these depth ranges start at surface as all eddies are strongly signed by circularly like surface currents and end at depth were anomalies are very weak), T20/850 dbar (baroclinic geostrophic transport at 20 dbar using a reference depth at 850 dbar and geopotential differences between "in" and "out" casts. For eddies A and B, this is only slightly less when using 1500 dbar. Numbers inside brackets for eddy B refer to the transport corresponding to depths between 20 and 250 dbar (B_{surf}) and between 250 and 850 dbar B_{deep}), ΔX (distance between the "in" cast and the "out" cast used as a reference to determine anomalies at constant depth. ΔH (depth deepening of the maximum anomaly isopycn $\sigma^{E_{MaxAno}}$ from "out" to "in" casts (see Supplement). Characteristics of the anomalies: Anomaly is the difference at constant depth between "in" and "out" profiles for the selected parameter, ^{E} is for anomaly eddy. $D^{E_{TopAno}}$ (depth of the top of anomaly, i.e. that anomaly weakens upwards), $D^{E_{MaxAno}}$ (Depth where the absolute anomaly is maximum), $D^{E_{BotAno}}$ (depth of the bottom of anomaly, i.e. that anomaly weakens downwards). The depths recorded here were taken with excess density σ, but some weak variations were observed for other parameter, σ^{E}_{MaxAno} (excess density at $D^{E_{MaxAno}}$), $S^{E_{MaxAno}}$ (ibid for salinity), θ^{E}_{MaxAno} (ibid for Potential Temperature), $AOU^{E_{MaxAno}}$ (ibid for AOU), $\delta\sigma^{E}$ (anomaly in excess density observed at $D^{E_{MaxAno}}$), δS^{E} (ibid for Salinity), $\delta\theta^{E}$ (ibid for Potential Temperature), δAOU^{E} (ibid for AOU). Dynamical Characteristics: δG_{Max} (maximum value of geopotential difference as observed between "in" and "out" profiles using a reference depth at 850 dbar), DG_{Max} (Depth of δG_{Max} and Vaz_{Max}), Vaz_{Max} (depth azimuthal velocity maximum; by convention the azimuthal velocity is negative in an anticylonic eddy, Vaz_{Max} is inferred from VMADCP), $rVaz_{Max}$ (distance on an eddy diameter between the 2 Vaz_{Max}. This distance should correspond to $L\sqrt{2}$ where L is the Rayleigh distance (see Supplement)), ω(Tr) (rotation pulsation, also negative (number of days for one complete rotation)), f(lat), (Coriolis parameter, latitude), ζ_{min}/f (ratio of the minimum relative vorticity occurring close to the eddy axis to the Coriolis parameter. This negative parameter, calculated as $2\omega/f$, indicates the strength of the eddy trough which isolates the eddy core in solid rotation from outside advection.

BGD
8, 8091–8160, 2011

Table 3.

Specific characteristics		LD Stations			
	Units	A	B_{surf}	B_{deep}	C
General					
D_{Bottom}	dbars	2758	3070	3070	923
D_{range}	dbars	0–420	0–250	250–1200	0–800
T20/850 dbars	Sv	2.40	3.45 (1.70)*	3.45 (1.75)*	3.04
ΔX	km	142	128	128	71
ΔH	m	91	70	330	231
Anomalies					
$D^{E_{TopAno}}$	dbars	90	95	300	120
$D^{E_{MaxAno}}$	dbars	160	135	600	380
$D^{E_{BotAno}}$	dbars	420	250	1200	800
σ^{E}MaxAno	kg m^{-3}	28.202	28.433	29.012	28.84
$S^{E_{MaxAno}}$	no dimension	37.68	38.44	38.96	39.39
$\theta^{E_{MaxAno}}$	°C	14.27	15.86	15.06	17.2
$AOU^{E_{MaxAno}}$	µmol kg^{-1}	13	5	21	12
$\delta\sigma^{E}$	kg m^{-3}	−0.66	−0.32	−0.134	−0.251
δS^{E}	PSU	−0.65	−0.28	+0.14	+0.388
$\delta\theta^{E}$	°C	0.75	0.5	1.04	2.35
δAOU^{E}	µmol kg^{-1}	−50	0	−30	−40
Integrated σ Ano (0–850 m)	kg m^{-2}	−20	–	−108	−48.2
Integrated S: (PSU) Ano (0–850 m)	m^{-2}	−126.1	–	28.3	111.4
Integrated θ Ano (0–850 m)	°C m	122		555	580
Integrated AOU Ano (0–850 m)	µmol m^{-2}	−9328	–	−9771	−7665
Dynamical Characteristics					
δG_{Max}	m^2 s^{-2}	1.26	0.42	0.98 (0.58)	0.65
DG_{Max}	dbars	40	30	30 (250)	90
Vaz_{Max}	ms^{-1}	−0.33	−0.20	?	−0.20
$rVaz_{Max}$	km	58	42.5	?	48
ω (Tr)	10^{-5} rad s^{-1} (days)	−1.8181 (4)	−1.212 (6)	?	−1.3222 (5.5)
f (lat)	10^{-5} rad/s (° N)	9.1531 (39.1)	8.1542 (34.1)	8.1542 (34.1)	8.0699 (33.7)
ζ_{min}/f	no dimension	−0.3973	−0.2973	?	−0.3277
$D^{E_{WML2008}}$	dbar	90.5	109.5	109.5	396.5
$D_{WML2008OUT}$	dbar	57.5	89.5	300*	153.5

BGD
8, 8091–8160, 2011

Table 4. Sediment trap data at the LD stations. Depth of collection, Mass flux in mg m^{-2} d^{-1} of matter DW and for each elements C, N and P. SD in italics.

Station	depth of collection m	Mass flux mg m^{-2} d^{-1}	PC mgC m^{-2} d^{-1}	PN mgN m^{-2} d^{-1}	PP mgP m^{-2} d^{-1}	C:N:P molar ratio 106:x;y
LD A	230	14.26	2.52	0.35	0.16	106:13:2.6
		1.29	*0.19*	*0.12*	*0.23*	
	460	16.61	1.68	0.31	0.19	106:11:3.2
		5.16	*0.54*	*0.22*	*0.16*	
LD B	230	26.26	2.54	0.45	0.06	106:16:1.0
		15.48	*0.99*	*0.20*	*0.03*	
	460	21.80	1.26	0.19	0.64	106:7:10.4
		24.57	*0.88*	*0.11*	*1.00*	
LD C	230	17.27	3.09	0.49	0.04	106:18:0.6
		7.93	*0.49*	*0.05*	*0.00*	
	460	19.40	2.26	0.49	0.02	106:18:0.4
		12.03	*1.29*	*0.31*	*0.02*	

BGD
8, 8091–8160, 2011

Table 5. Daily N budget at the three LD stations A, B, and C.

Specific characteristics	Units	LD Stations		
		A	B	C
D_{NO_3}	m	72	114	93
S_{NO_3}	$\mu mol\, m^{-4}$	11.8	15.5	24.9
Input by diffusion	$\mu mol\, m^{-2}\, d^{-1}$	10.1	13.3	21.4
Input by nitrogen fixation	$\mu mol\, m^{-2}\, d^{-1}$	12.5	15.2	0.2
Input of new nitrogen	$\mu mol\ m^{-2}\, d^{-1}$	22.6	28.5	21.6
N-budget export at 230 m	$\mu mol\, m^{-2}\, d^{-1}$	25.3	32.0	34.8
Integrated Gross Primary Production	$\mu mol\, m^{-2}\, d^{-1}$	3470	4130	3560
Export production	%	0.9	0.8	1.0
Regenerated production	%	99.1	99.2	99.0

BGD
8, 8091–8160, 2011

Table 6. Annual N-budget at the three LD stations A, B, and C.

Specific characteristics	Units	LD Stations		
		A	B	C
EZD	m	83	104	102
WML-D	m	90.5	109.5	396.5
$[NO_3]_{W\ ML}$	mmol m^{-3}	0.47 (100 m)	0.00 (124 m)	0.73 (348 m)
Input from previous winter convection	mmol m^{-2} y^{-1}	39.0	0.0	74.5
Input by diffusion	mmol m^{-2} y^{-1}	3.1	4.1	6.5
Input by nitrogen fixation	mmol m^{-2} y^{-1}	4.6	5.5	0.1
Annual input of new N	mmol m^{-2} y^{-1}	46.7	9.6	81.1
Winter convection	% of annual new N	83.5	0.0	91.9
Diffusion	% of annual new N	6.6	42.7	8.0
Nitrogen fixation	% of annual new N	9.9	57.3	0.1
Background export	mmol m^{-2} y^{-1}	9.2	11.7	12.7
"Spring" export	%	80.3	0.0	84.3

BGD
8, 8091–8160, 2011

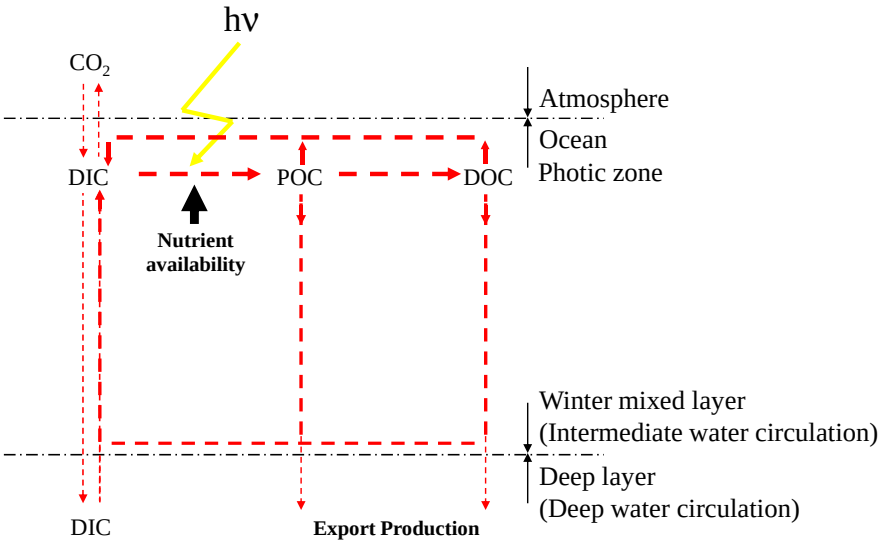

Fig. 1. Biological pump: carbon transfer by biological processes into the ocean interior. Modified from Moutin et al. (2000).

BGD
8, 8091–8160, 2011

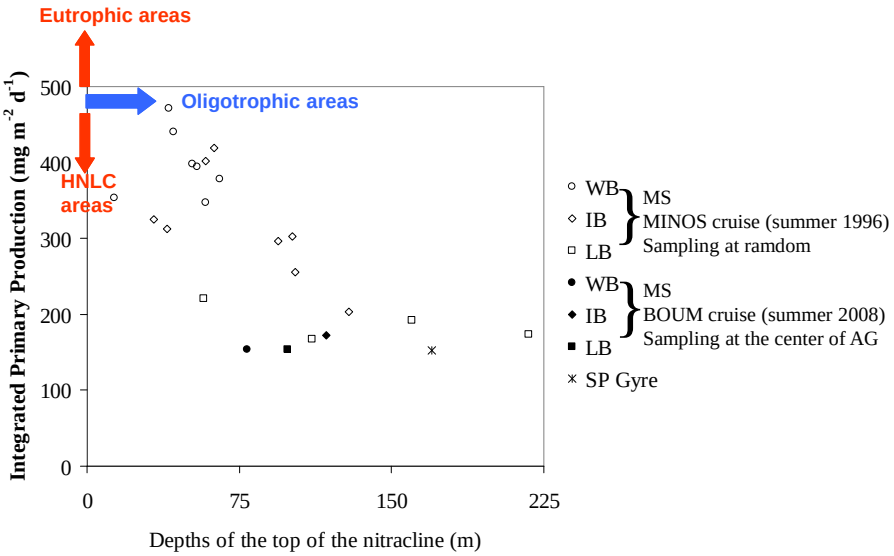

Fig. 2. Integrated Primary Production vs. depth at the top of the nitracline. Data from the MS in the Western Basin (WB), the Ionian Basin (IB) and the Levantin Basin (LB): MINOS cruise (Moutin and Raimbault, 2002) and BOUM cruise, and data from the most oligotrophic area in the world ocean, the South Pacific gyre (T. Moutin, unpublished data).

BGD
8, 8091–8160, 2011

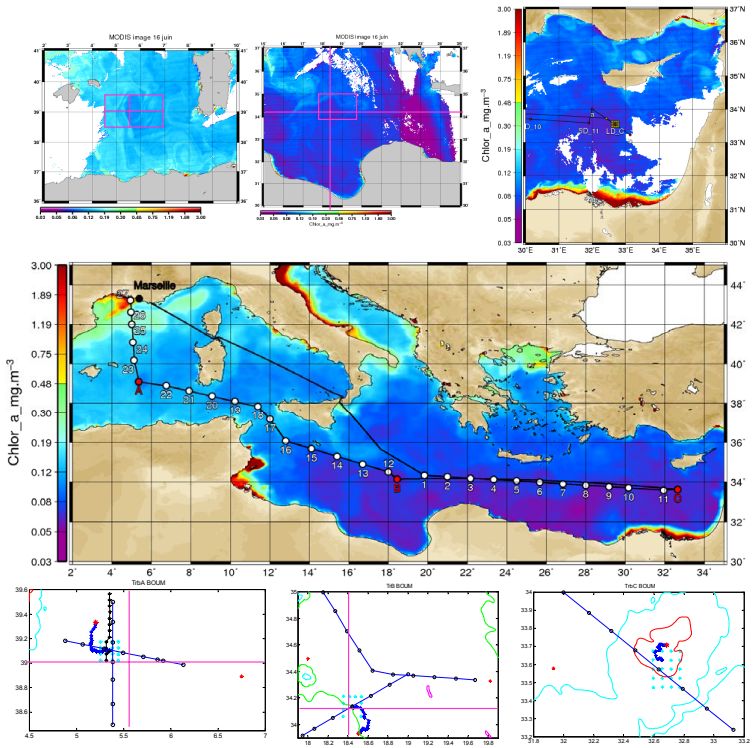

Fig. 3. Middle: transect of the BOUM cruise superimposed on a SeaWiFS composite image of chl-*a* concentration in the upper layer of the MS between 16 June and 20 July 2008. The two types of station, short duration and long duration, are indicated. The three LD stations investigated for a period longer than four days are indicated in red and are located in the centre of an anticyclonic eddy (courtesy of E. Bosc). Top: small size colour images indicating the location of eddies previous to sampling and small displacements of the eddies through comparison with the image below. Bottom: XBT survey (black circles) and sampling grid stations (blue crosses) investigated to locate eddy centres.

BGD
8, 8091–8160, 2011

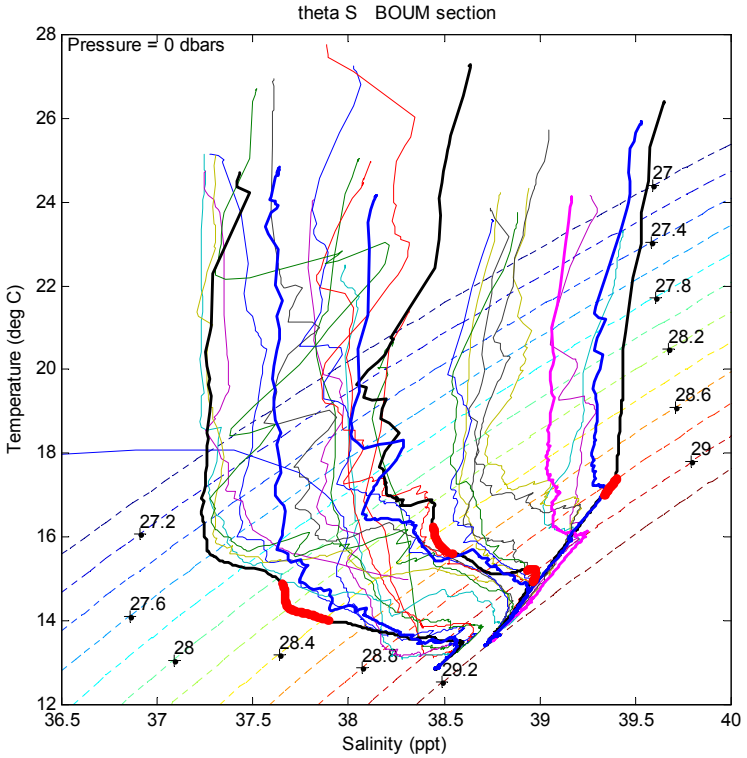

Fig. 4. Theta S diagrams of each station during the BOUM cruise transect. The colour lines represent the SD stations and the thick lines the LD stations, A, B, and C from left to right. Labels of density isolines (dotted lines) are expressed as excess density above 1000 kg m^{-3}, considering a pressure reference at 0 dbar. Graph realized with the matlab Woods Holes routine (WHOI toolbox). Depths between the top and maximum anomalies (defined Sect. 5.4) are represented in thick red, and the "out" profiles (same section), chosen to characterize each eddy (casts 17, 2 and 130 for eddy C, B and A, respectively), are shown in thick blue.

BGD
8, 8091–8160, 2011

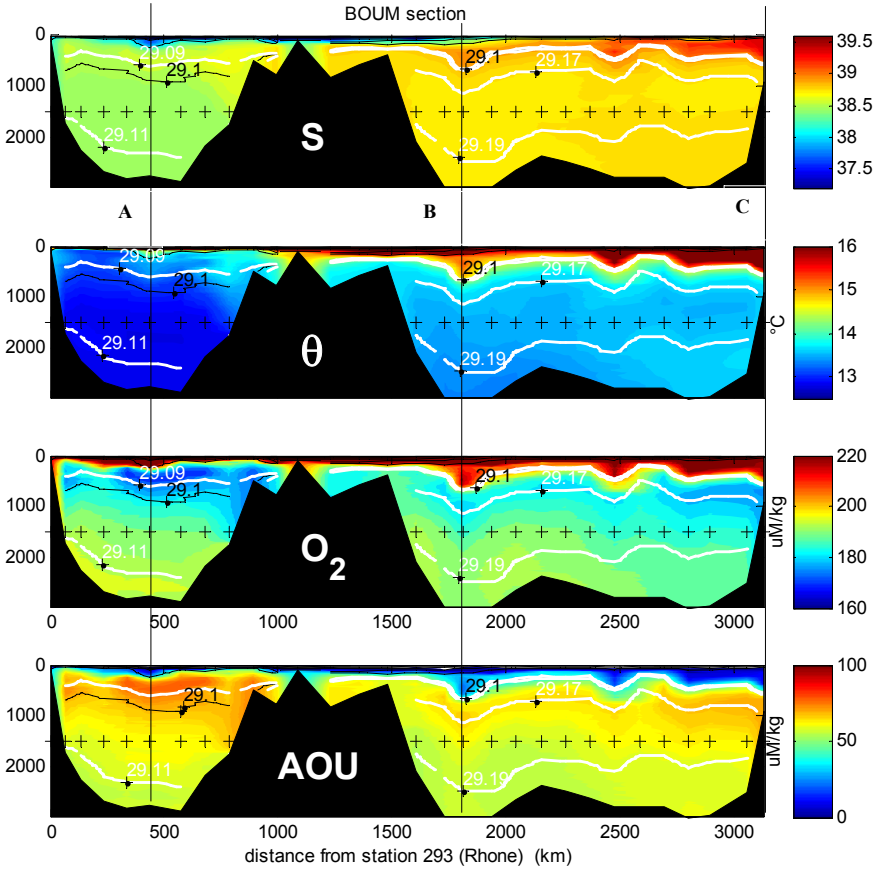

Fig. 5. Salinity (S, PSU), potential temperature (°C), oxygen concentration and Apparent Oxygen Utilization (µmol kg^{-1}) sections along the BOUM transect (0–3000 dbar) from the Rhône river mouth in the western part of the MS to the Eratosthenes Seamount in the eastern part. Black vertical lines indicate the location of the 3 LD stations A, B, C.

BGD
8, 8091–8160, 2011

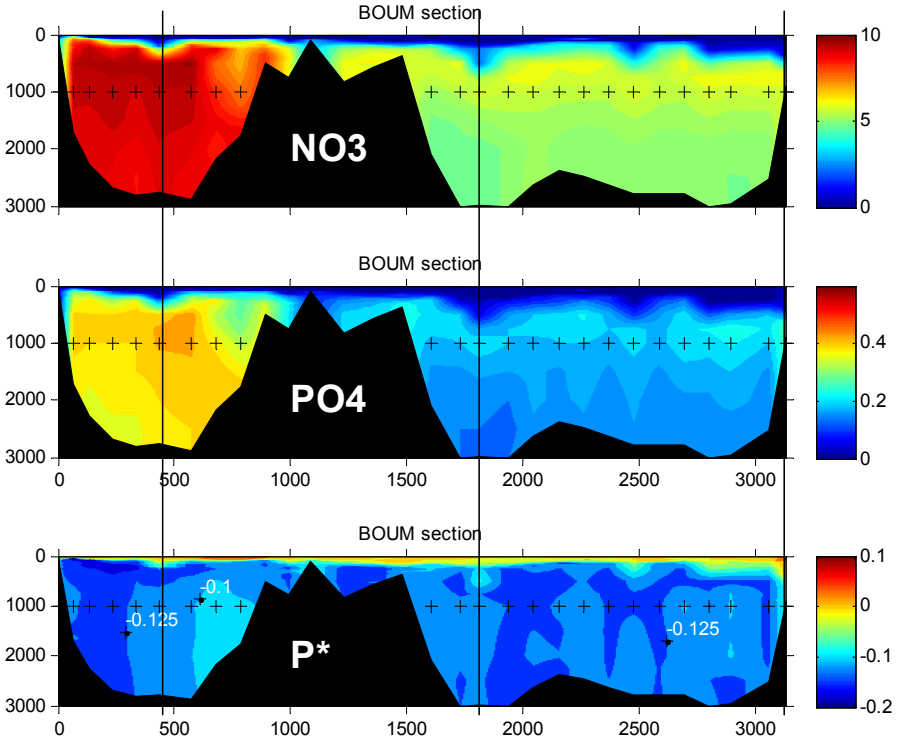

Fig. 6. Nitrate and phosphate concentrations (μM) and P^* (μM) sections along the BOUM transect (0–3000 dbar). $P^* = NO_3\text{-}PO_4/Rr$; $Rr = 17.7$ following Pujo-Pay et al. (2011). Linear interpolation between bottle data each 10 dbar was used to generate the distribution maps. Black vertical lines indicate the location of the three LD stations A, B, C.

BGD
8, 8091–8160, 2011

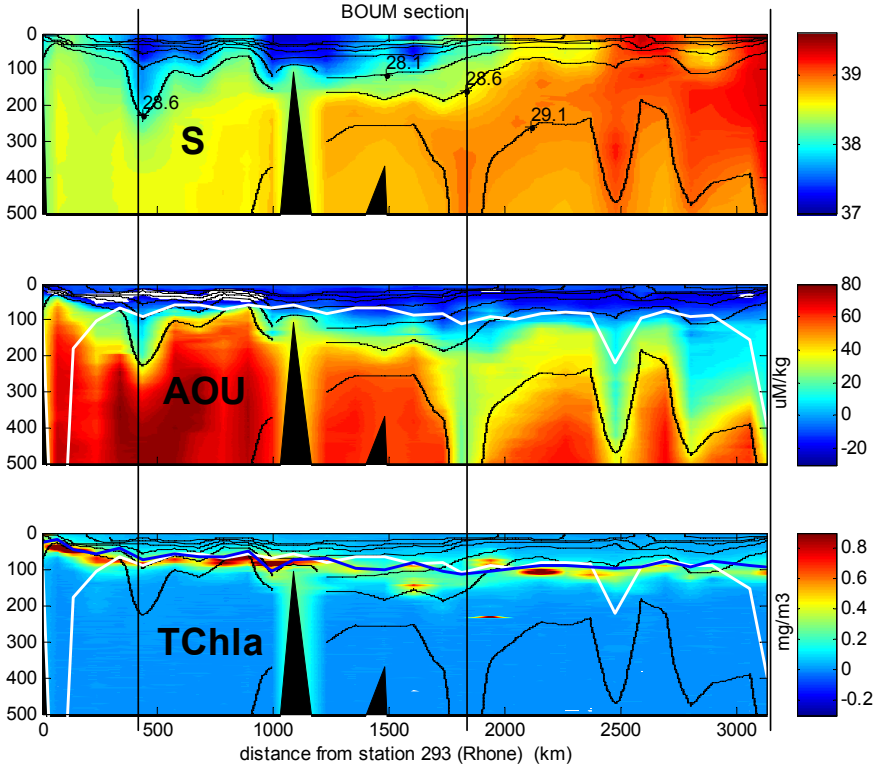

Fig. 7. Salinity (S, PSU), Apparent Oxygen Utilisation (micromol kg-1) and Tchlo-a ($\mu g\, l^{-1}$) sections along the BOUM transect (0-500 dbar). Black vertical lines indicate the location of the three LD stations A, B, C.

BGD
8, 8091–8160, 2011

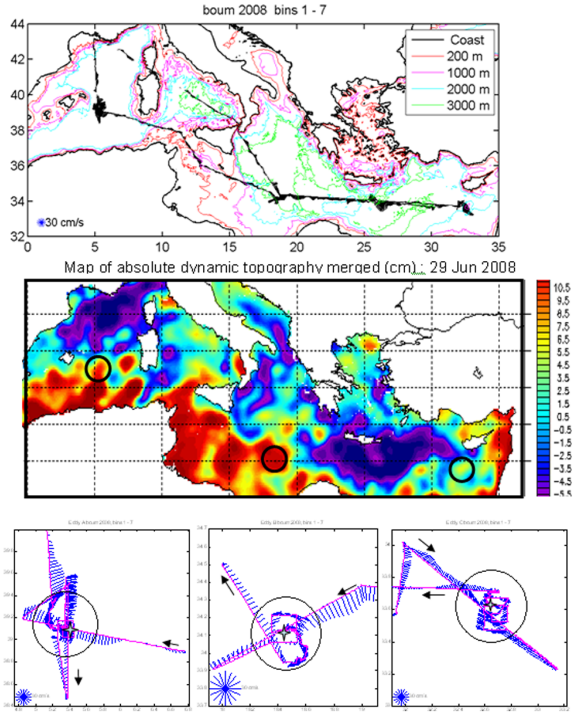

Fig. 8a. Top: map of the bathymetry (GEBCO 1998) together with the mean velocities measured with the ship ADCP along the transect between 29 and 125 m depth (scale is indicated in blue in the lower left corner). Middle: map of the sea surface Dynamic Topography obtained from AVISO on 2008 June 29th and redrawn in Mercator coordinates (colour scale in cm). Location of each eddy is indicated by a black circle around the local maximum. Bottom: Details of ship course (pink) and mean ADCP currents measured around the three eddies, A, B, and C. Ship ADCP vectors are drawn each 10 min of cruise time from vessel location (Velocity scales are indicated in the left corner of each map). The circles of diameters $dVaz_{max}$ are positioned at the centre location of each eddy (shown by stars), as estimated before the beginning of LD stations.

BGD
8, 8091–8160, 2011

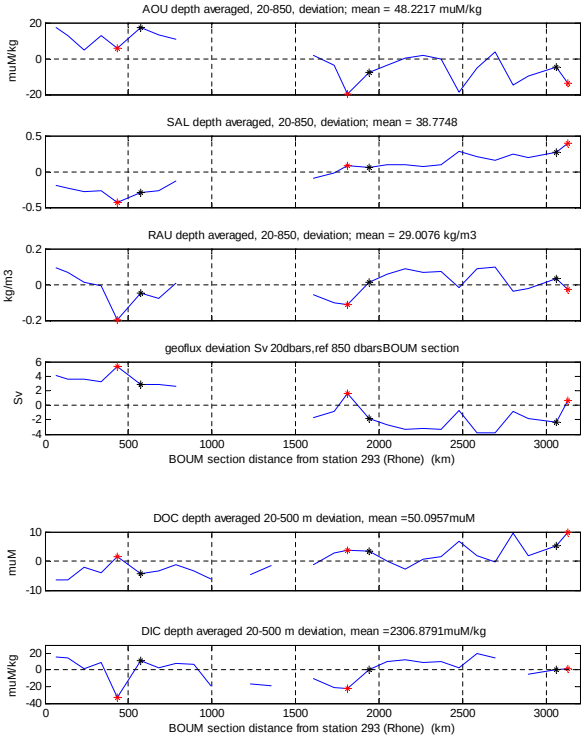

Fig. 8b. Deviation between depth-averaged (20–850 dbar) values and the mean depth-averaged values for the whole transect of: AOU (µmol kg^{-1}); Salinity (PSU); excess density (kg m^{-3}); geoflux function (Sv) and the differences between baroclinic geostrophic transports at 20 dbar when considering a reference at 850 dbar (0 Sv); Dissolved Organic Carbon (DOC µmol kg^{-1}) and Dissolved Inorganic Carbon (DIC µmol kg^{-1}) along the BOUM transect. Mean(AOU) = 48.222 µmol kg^{-1}, Mean(S) = 38.775, Mean(excess density) = 29.0076 kg m^{-3}). The positions of eddies A, B, and C are indicated with red crosses and the positions of casts are indicated by black crosses. No values were obtained when bottom depths were <850 dbar, as occured near the Rhone river mouth and in the Sicilian Channel.

BGD
8, 8091–8160, 2011

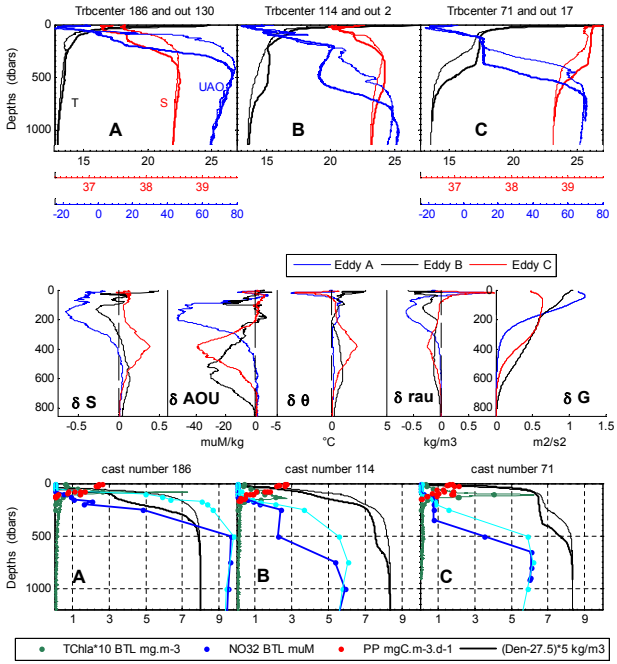

Fig. 9. Top: vertical profiles of potential temperature (°C in black), salinity (PSU in red) and AOU (µmol kg^{-1} in blue) vs pressure (0–1500 dbar) inside the eddies (thick lines; casts 186, 114 and 71 for LD stations A, B and C, respectively) and outside but from the closest SD station (thin lines; casts 130, 2 and 17). The same scales for each LD station A, B, and C with the corresponding colours are reported below. Middle : Vertical profiles of S, AOU, $\theta\rho$ and G anomalies from left to right. Depths of top and bottom anomalies indicated in Table 3 are clearly shown. Bottom: Vertical profiles of primary production (o: mgC m^{-3} d^{-1}), Total chl-*a** 10 (green $_*$ for HPLC measurements and – for fluorescence converted measurements: µg l^{-1}) and density ((ρ-27.5)*5, –: kg m^{-3}), vs pressure (dbar) at the three LD stations (same casts as for Fig. 9 (top) but with rosette sampling except for density). Primary production was measured twice during the LD station occupation. Vertical profiles of nitrate concentration (µmol kg^{-1}) vs pressure inside (dark blue $*$) and outside (light blue $*$) the eddies for the same cast and station as for AOU in the top figure.

BGD
8, 8091–8160, 2011

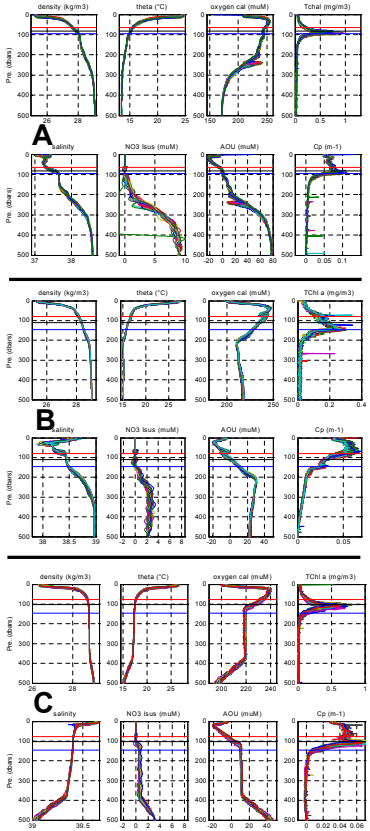

Fig. 10. Superposition of all vertical profiles vs. depth (0–500 dbar) obtained during occupation of the LD stations A, B, and C in uppermost position and from left to right: excess density (kg m^{-3}), potential temperature (°C), dissolved oxygen (µmol kg^{-1}), total chl-*a* (mg m^{-3}), and in lower position: Salinity (PSU), ISUS nitrate concentration (µM), AOU (µmol kg^{-1}) and *Cp* (m^{-1}). The best X-axis scale is chosen for each stations. The 3, 1 and 0.3 % of incident light level were reported on each graph using horizontal lines in red, green and blue, respectively.

BGD
8, 8091–8160, 2011

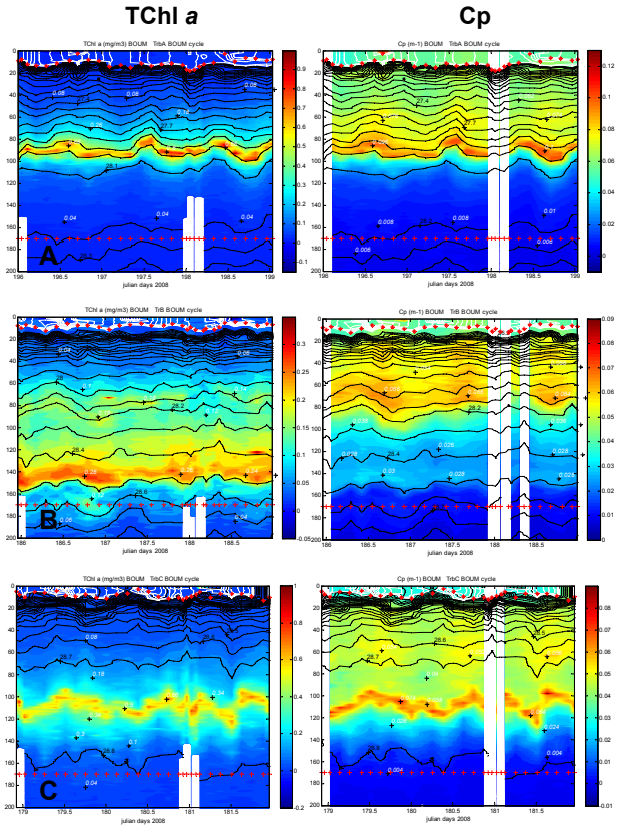

Fig. 11. Temporal sections between 0–200 m depth for tchl-*a* (mg m^{-3}) and for the optical attenuation coefficient *Cp* (m^{-1}) for the particles at the LD stations A (top), B (middle) and C (bottom). The dates on the X-axis are in 2008 Julian days and the dates of the profiles are indicated by red cross near 170 dbar. The red stars indicate $MLD_{0.03}$.

BGD
8, 8091–8160, 2011